(NASA-TM-X-68726) INTERACTION OF GRAPHITE AND ABLATIVE MATERIALS WITH CO2-LASER, CARBON-ARC, AND XENON-ARC RADIATION M.S. Thesis - George Washington Univ., Washington, D. C. (NASA) 81 p HC $4.75 G3/24

N75-22385

Unclas 20245

Interaction of Graphite and Ablative Materials with CO_2-laser, Carbon-arc, and Xenon-arc Radiation

by

William Dennis Brewer

B.S. June 1962, Wake Forest University

A Thesis submitted to

The Faculty of

The Graduate School of Engineering and Applied Science

of the George Washington University in partial satisfaction

of the requirements for the degree of Master of Science

May 1975

ACKNOWLEDGMENTS

The author acknowledges the National Aeronautics and Space Administration for permission to use, in this thesis, material obtained from research conducted at the Langley Research Center. Appreciation is expressed to Dr. John D. Buckley for serving as thesis advisor and for his comments and suggestions during the preparation of this thesis.

ABSTRACT

Results are presented from an investigation of the behavior of graphite and several charring ablators in a variety of high radiative heat-flux environments. A commercial grade graphite and six state-of-the-art charring ablators were subjected to various radiative environments produced by a CO_2 laser and a carbon-arc facility. Graphite was also tested in xenon-arc radiation. Heat flux levels ranged from 10 to 47 MW/m^2. Tests were conducted in air, nitrogen, helium, and a mixture of CO_2 and nitrogen, simulating the Venus atmosphere. The experimental results are compared with theoretical results obtained with a one-dimensional charring ablator analysis and a two-dimensional subliming ablator analysis. Photomicroscopy showed no significant differences in appearance or microstructure of the charring ablators or graphite after testing in the three different facilities, indicating that the materials responded fundamentally the same to the radiation of different frequencies. The performance of phenolic nylon and graphite was satisfactorily predicted with existing analyses and published material property data. Good agreement between experimental and analytical results was obtained with sublimation parameters from a chemical non-equilibrium analysis of graphite sublimation. Some charring ablators performed reasonably well and can satisfactorily withstand radiative fluxes of the level encountered in Venus entry. Other materials showed excessive surface recession and/or large amounts of cracking and spalling and appear to be unsuitable for the severe radiative environments.

TABLE OF CONTENTS

LIST OF TABLES

LIST OF FIGURES

LIST OF SYMBOLS

A_c	constant in oxidation equation corresponding to specific reaction rate
A_s	constant in sublimation equation
B_c	constant in exponent of oxidation equation corresponding to activation energy
B_s	constant in exponent of sublimation equation
C_e	oxygen concentration at edge of boundary layer
C_w	oxygen concentration at wall
c_p	specific heat
$\bar{c}_p$	specific heat of pyrolysis gases
E	ablative effectiveness parameter
h_e	enthalpy external to boundary layer
h_w	enthalpy at wall
h_1, h_2, h_3	coordinate scale factors
ΔH_c	heat of combustion
ΔH_p	heat of pyrolysis
ΔH_s	heat of sublimation
K	reaction rate constant for oxidation
k	thermal conductivity
Δl	interface recession
Δm	mass loss

$\dot{m}$	mass loss rate
$\dot{m}_c$	rate of char loss
$\dot{m}(O_2)$	rate at which oxygen diffuses to the surface
$\dot{m}_p$	rate of loss of uncharred material
$\dot{m}_s$	mass loss rate due to sublimation
p	exponent of pressure in sublimation equation
P_w	pressure at wall
q_c	convective heat flux to cold wall
$q_{c,net}$	net convective heat flux to ablating hot wall
q_n	net radiative heat flux-experimental
q_{net}	net heat flux to surface
q_r	radiative heat flux to surface
R	radius of test sample
R_{stag}	stagnation point radius of curvature
r	exponent of radius in sublimation equation
s	distance along radius from center of test sample
T	temperature
T_b	temperature to which back surface is radiating
T_w	temperature of wall
t	test time
Δx	surface recession-experimental
x,y	coordinates
x_b	length of base curve (Figure 8)
$\bar{x}$	surface recession (Figure 7)
α	absorptance

α_c	weighting factor for transpiration effectiveness of mass loss due to combustion
α_s	weighting factor for transpiration effectiveness of mass loss due to sublimation
β	0 or 1 depending on whether transpiration or ablation theory is used
γ	absorption coefficient
δ	thickness of material
ϵ	emittance
ζ	ratio of molecular weight of gas to molecular weight of oxygen
λ	mass of char removed per unit mass of oxygen
ξ,η	dimensionless curvilinear coordinates (equations (15))
ρ	material density
σ	Stephan-Boltzmann constant
τ	time

Superscripts

'	indicates uncharred material
c	corrected for reduced heat flux

I. INTRODUCTION

Charring ablative materials as well as graphite have been used to protect space vehicles from the heating environment encountered when reentering the earth's atmosphere from space. The performance of these materials subjected to environments such as those experienced in earth reentry at orbital and escape velocity has been extensively investigated (refs. 1, 2, 3). Various types of analyses have been developed to predict the behavior of materials in such environments (refs. 4-9). For proposed planetary missions, however, it becomes necessary to reexamine the problems of protecting the reentry vehicles from the severe heating. Atmospheric entry in such missions is characterized by large radiative as well as convective heat inputs to an entry vehicle. In spite of recent emphasis on the study of these missions, there is still a need for a better understanding of the interaction of the planetary entry type environments with thermal protection systems. It is of prime importance to know how a material responds to various types and levels of heating and whether or not existing analyses can be used to predict material performance in the various heating regimes.

Flight tests of each promising thermal protection material are not feasible for obvious reasons, and the present capability for simulating planetary entry environments in ground-based facilities is limited. There are facilities capable of producing radiative and convective heating of the appropriate levels for simulating some planetary entry conditions, for example, selected entries into the Venus

atmosphere. However, other parameters such as the spectral distribution of the radiation and the type of atmospheric gases are in general, not well simulated. High power lasers are the only convenient sources which at present can produce heat fluxes approaching those expected in entry into the major planets. The spectral distribution of radiation produced in these lasers is quite different from that in an actual reentry situation and the behavior of materials could conceivably be different. It is therefore necessary to examine material response to a variety of environments.

A program was undertaken to investigate the behavior of graphite and several charring ablators in various radiative heating environments. The objectives of the program were: (1) to investigate the important ablative mechanisms and how they are affected by a change in environment. (2) to investigate ablative mechanisms which may manifest themselves under planetary entry type conditions and which are not taken into account by present thermochemical analyses. (3) to determine whether or not existing ablative analyses can be used satisfactorily to predict material performance in the different environments. (4) to determine the relative performance of some charring ablators in severe radiative environments.

To carry out this program, a commercial grade graphite and six state-of-the-art charring ablators were subjected to radiative heating environments produced by a CO_2 laser, a carbon arc, and a xenon arc. The heat flux levels produced by these facilities are comparable, although the characteristics of the radiation are significantly different.

The experimental results obtained from these tests were compared to theoretical results obtained with the use of two different computer programs which treat the transient response of charring and subliming ablators to heating environments.

II. MATERIALS

The materials investigated in the laser experiments are as follows:

1. A phenolic-carbon (PC) composite of 50% phenolic resin and 50% carbon fibers, with a density of 1450 kg/m^3. (All percentages are by weight.)

2. A high density phenolic nylon (HDPN), composed of 50% phenolic resin and 50% nylon powder. The density is 1200 kg/m^3.

3. A low density phenolic nylon (LDPN) composed of 25% phenolic resin, 25% phenolic Microballoons, and 50% nylon powder (density = 550 kg/m^3).

4. A silicone elastomer, 75% silicone resin, 15% SiO_2 in the form of tiny hollow spheres (11%) and fibers (4%), and 10% phenolic Microballoons. The density is 640 kg/m^3.

Materials 1-4 are discussed in more detail in references 2 and 10.

5. A filled epoxy material (Apollo heat shield material) the composition of which is proprietary. Some measured material properties are given in reference 10. The density is 500 kg/m^3.

6. A 500 kg/m^3 polybenzimidazole (PBI) which is 69% PBI prepolymer, 13% carbon fibers and 18% phenolic Microballoons (material 5, reference 11).

7. A commercial-grade, fine-grained graphite with a density of 1800 kg/m^3.

The materials tested in the carbon-arc experiments were the graphite, low density phenolic nylon, filled epoxy and silicone elastomer used in the laser tests. In addition, 3 types of pyrone (developed at Langley Research Center) were tested in the carbon arc. The materials are designated P-1, a glass-filled pyrone resin with a density of

600 kg/m^3; P-2, a foamed pyrone with a density of 680 kg/m^3; and P-3, an uncured pyrone resin with a density of 480 kg/m^3. Only the graphite was tested in the xenon arc.

III. EXPERIMENTAL APPARATUS AND PROCEDURES

Tests were conducted with three different radiation sources; a CO_2 laser, a carbon arc, and a xenon arc. The spectral distributions of the radiation from these sources are shown in Figure 1. Figure 1 also shows typical shock layer radiation spectra for two planetary atmospheres; Earth (air and ablation products) and Venus (CO_2 - N_2). The radiation from the xenon-arc facility and the carbon-arc facility covers a significant portion of the Venus and Earth reentry spectral range. The laser radiation is considerably different from either of the other sources. In addition to being highly coherent and monochromatic, the radiation produced by the laser is out of the spectral range of the actual reentry environments. Details of the test apparatus and procedures are given in the following sections.

Laser Experiments

Test Apparatus - The laser used in these experiments was a continuous, d-c excited, flowing-gas, CO_2 - N_2 - H_e laser. The maximum power output of the device is about 9 kW. For the tests discussed here the laser was operated at about 6 kW with a beam diameter of 4.4 cm. The design, construction and operating characteristics of the laser are discussed in detail in reference 12.

The test set-up used for the present experiments is shown schematically in Figure 2. The parallel beam emerged from the laser tube, was reflected by a segmented mirror through a lense onto the surface of a sample located in a test chamber. The energy distribution

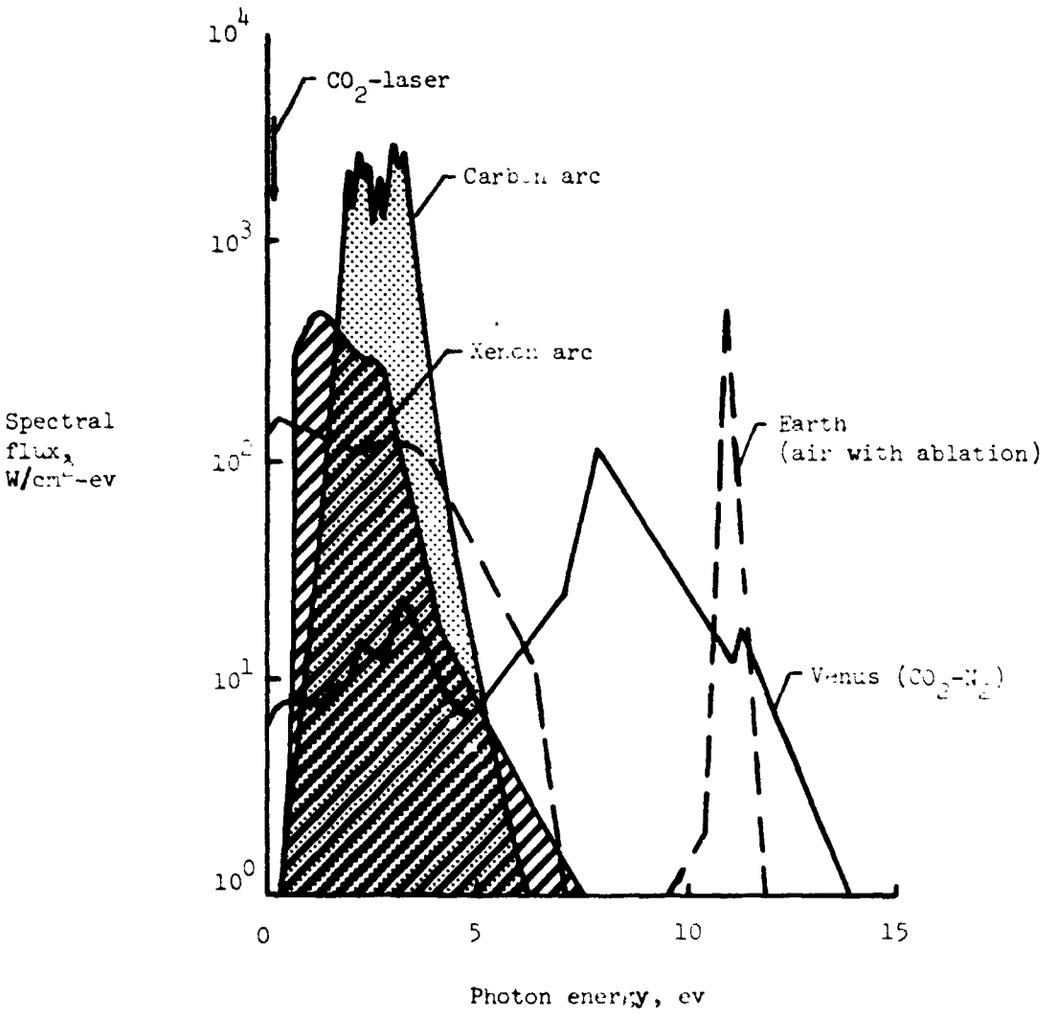

Figure 1.- Comparison of shock-layer spectra for earth and venus atmospheres with spectra for ground test facilities.

across the laser beam as it emerged from the tube was somewhat irregular and tended to have a sharp spike near the center, typical of high power laser systems. The segmented mirror was used to randomize or scramble the beam to produce a more nearly uniform and stable distribution across the surface of the samples. The mirror was a close-packed array of .95 cm diameter circular flats. The surfaces of the flats were set at appropriate angles so that the array approximated a parabolodial surface of 2m focal length. After reflection from the mirror, the beam passed through a circle of minimum focus of about 1.3 cm diameter at a point 2m from the mirror. The segmented mirror produced random interference effects and hence the intensity distribution at the focal plane was relatively insensitive to the distribution at the laser exit. The NaCl lense refocused the beam at a point about 16 cm from the test sample. The beam was therefore slightly divergent at the sample and hence minimized the heating of the sides of the samples. A retractable mirror was used to switch the beam from the sample optics to a calorimeter for calibrating the system. The mirror was controlled by an electric timer and was used to initiate and terminate sample exposure to the laser radiation.

A four-port test chamber used to enclose the test samples to provide a controlled environment. Visual observations, motion pictures, and sample temperature measurements were made through the side ports. The laser beam passed through a NaCl window on the front port, passed through a 1.3 cm diameter nozzle, and impinged on the sample surface. The test gas was injected into a plenum chamber and then flowed through

ORIGINAL PAGE IS
OF POOR QUALITY

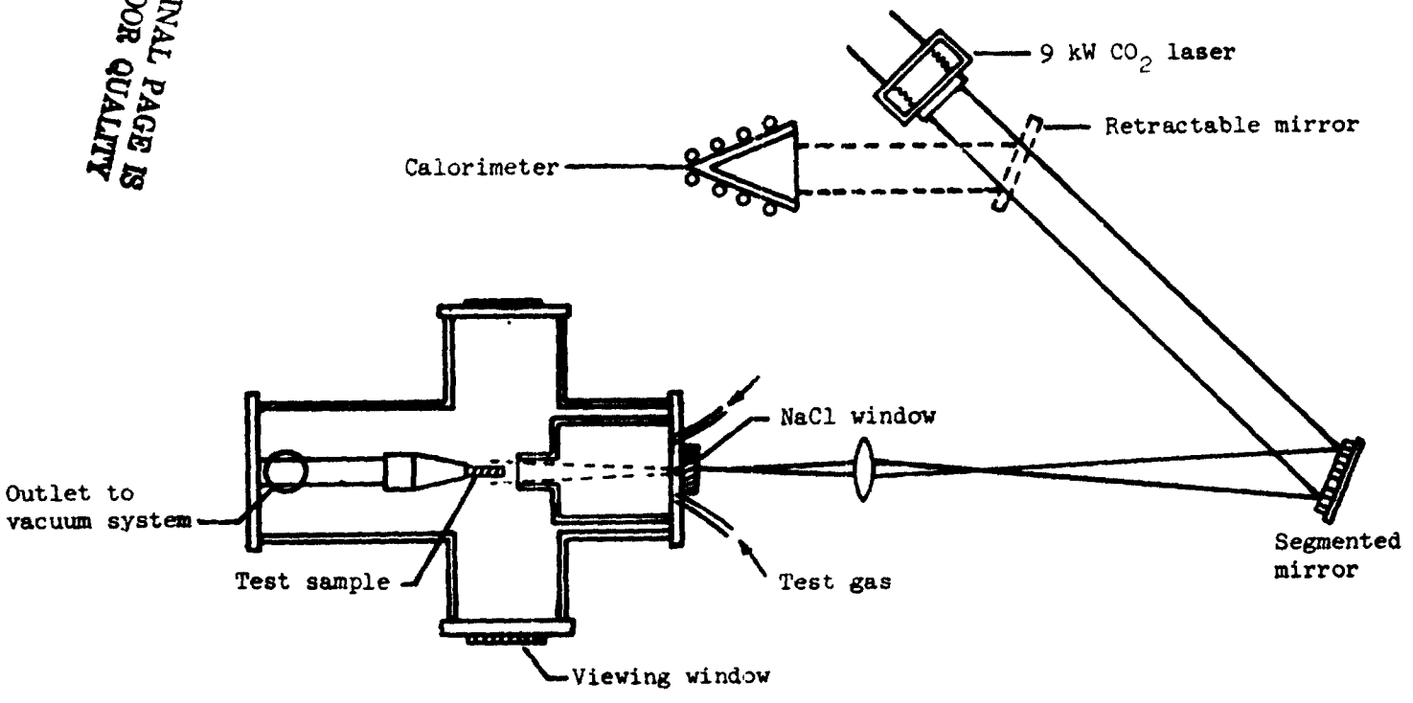

Figure 2.- Test set-up for laser experiments.

the nozzle and past the sample. The vacuum system connected to the rear port removed the test gas and the ablative products and controlled the pressure in the test chamber.

Instrumentation and calibration - Gas flow rates were measured with standard precision-bore flow meters. The pressure inside the test chamber was controlled by the vacuum system and was measured by conventional pressure gages.

An optical pyrometer responding to .65 μm radiation, was used to measure the temperature of the test samples. Because it was not possible to view the front surface of the samples, the temperature was measured on the side of the samples as close to the front surface as possible. The pyrometer was calibrated to account for the absorption of radiation by the glass viewing window.

Water cooled calorimeters were used to measure the power output from the laser and the power input to the samples. One calorimeter, called the primary calorimeter, measured the total power of the beam at the laser exit (Figure 2). Another calorimeter was placed at the rear of the test chamber to measure the total power after the beam had been attenuated by the optical system. The intensity distribution across the beam at the test location was determined by exposing polystyrene rods to the laser beam. The rods were sectioned after 0.1 - 1 second exposure and the intensity profiles were determined by the shape of the holes burned into the rods. This technique was validated by a point-by-point measurement of the power density across the diameter of the beam. The system was calibrated so that only a measurement of the

beam power at the laser exit was required to determine the maximum heat flux to the sample.

Test samples, conditions, and procedures - The laser test samples were 0.64 cm diameter cylinders 7.6 cm long. During the tests they were positioned so that about one-third of the length extended out of the holder. Test sample configurations are shown in Figure 3. The maximum heat fluxes to the sample ranged from 36 to 47 MW/m^2. However, the heating was not uniform over the surface of the samples. The heat flux at the edge of the samples ranged from 70 to 80 percent of the maximum, depending upon the power output of the laser. A typical heat flux distribution is given in Figure 4.

The gas flow rates were small ($\approx$ 30 m/s) but were sufficient to remove the ablation products from the area of the sample. The flow was uniform and stable throughout each tests. Test gases used were air, nitrogen, and helium.

The samples were placed in the test chamber and the system was regulated to obtain the desired gas flow rate and pressure. The laser was brought to the operating conditions with the retractable mirror reflecting the beam into the primary calorimeter (Figure 2). When the laser had stabilized, the power output was recorded, the mirror was removed from the path of the beam, and the sample was exposed to the laser radiation. At the end of the test, the mirror was again inserted into the path of the beam and another power measurement was made to determine whether or not the laser output had changed during the test. Each sample was measured and weighed before and after each test to

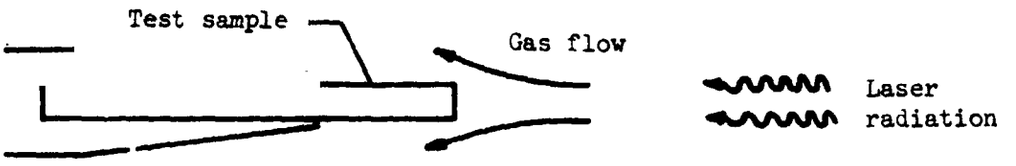

(a) Laser

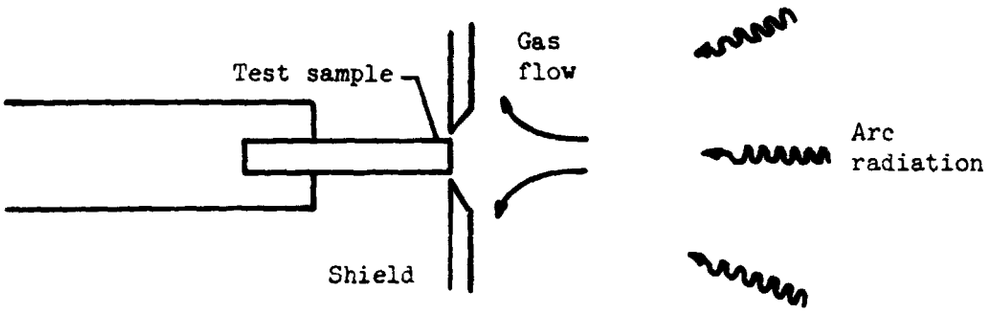

(b) Carbon arc

ORIGINAL PAGE IS
OF POOR QUALITY

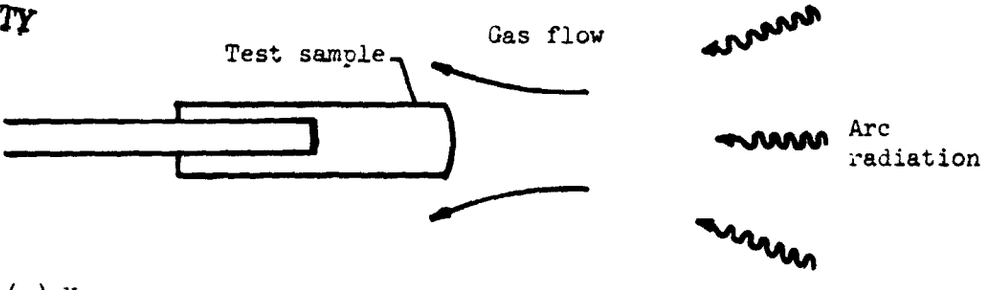

(c) Xenon arc

Figure 3.- Test-sample configurations for laser, carbon-arc and xenon arc experiments.

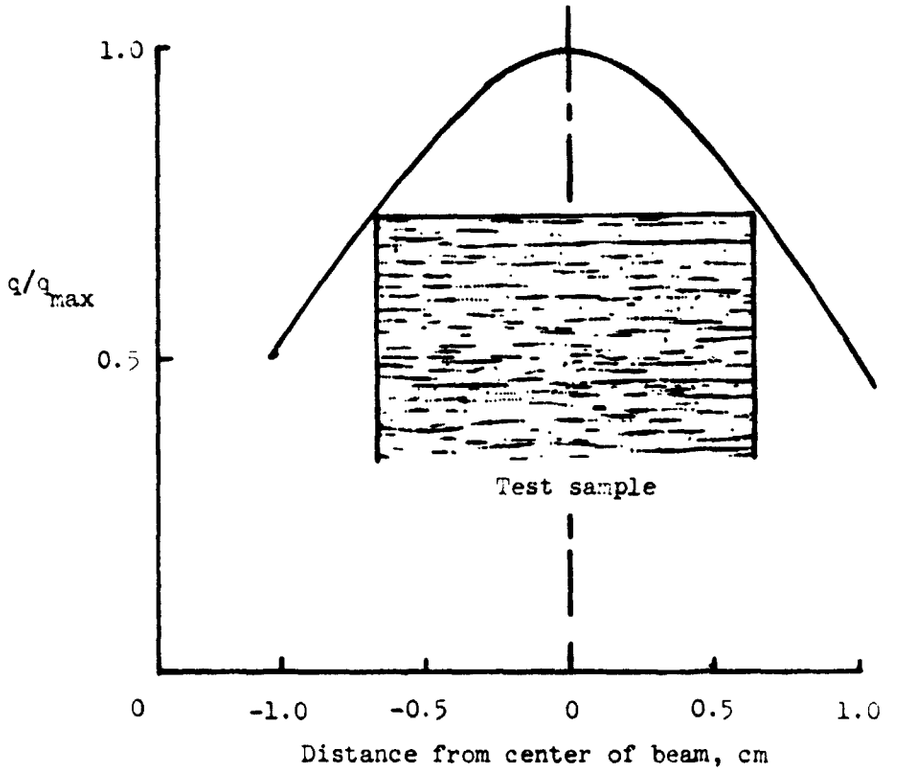

ORIGINAL PAGE IS
OF POOR QUALITY

Figure 4.- Typical heat-flux distribution in laser facility.

determine the surface recession and mass lost. To obtain significant recession, the graphite models were tested for 5 seconds; all others were tested for 2 seconds.

Carbon-Arc Experiments

Test apparatus - The tests in carbon-arc radiation were conducted in the arc-image facility at Southwest Research Institute. The operating characteristics are given in some detail in reference 13. A schematic diagram of the facility as used in this study is shown in Figure 5. The radiation from a carbon arc is collected and focused onto a test sample by twin parabolic mirrors. The front mirror has a hole, and the door to the facility has a quartz window for viewing the sample during testing. Motion pictures and surface temperature measurements are made through these windows. The test sample is enclosed in a small chamber so that the environment can be controlled independently of that in the arc chamber. A hemispherical quartz dome forms the front of the test chamber so that the radiation can be focused onto the sample. It was necessary to place a shield in front of the sample to eliminate radiation to the sides of the sample (Figure 3). The test gases are injected through a 1.3 cm diameter nozzle at a velocity of about 30 m/s, flow past the sample surface and are exhausted at the rear of the chamber.

A clam-shell type shutter was located directly in front of the sample to block all radiation while the arc facility was being brought to the desired operating conditions. The shutter was controlled by an electronic timer. Opening and closing times for the shutter were about 0.001 second.

ORIGINAL PAGE IS
OF POOR QUALITY

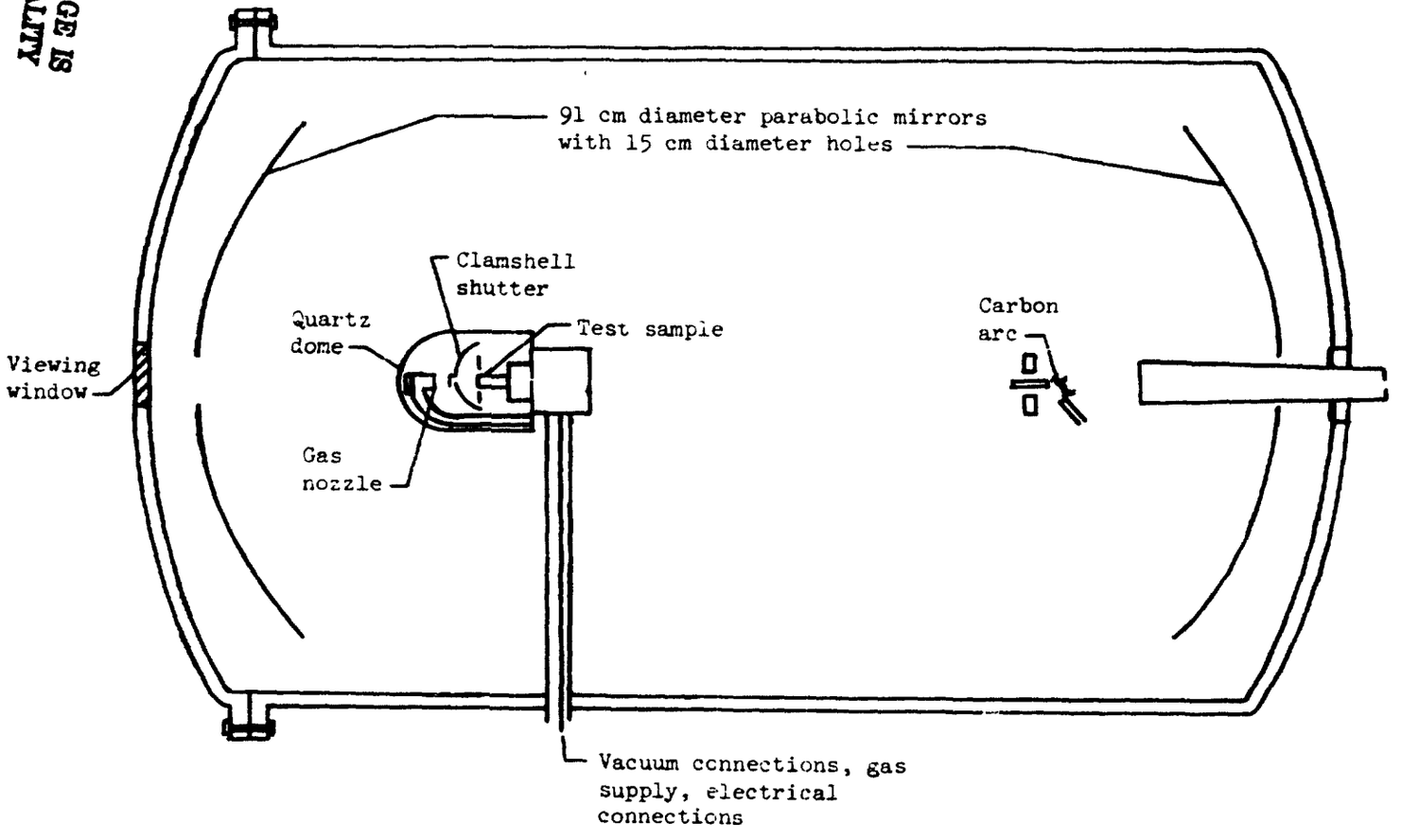

Figure 5.- Test set-up for carbon-arc experiments.

Instrumentation and calibration - The heat flux at the sample location was measured with a water-cooled, spherical-cavity, black-body calorimeter. During a calibration run, the calorimeter was placed behind the same shield as the sample so that only the radiation that would be incident on the sample surface was collected by the calorimeter. A correlation was made of the flux measured by this primary calorimeter with that measured by an asymptotic calorimeter located in the beam between the two parabolic mirrors. During a test, only the output of the asymptotic calorimeter was recorded. The heat flux to the sample was determined from these data.

The spatial distribution of the heat flux was determined by placing a block of sodium silicate at the sample location and exposing it to the arc radiation. After the block was exposed to the test environment, it was sectioned and the heating distribution was determined from the shape of the hole burned into the block. In the carbon-arc facility, the variation in heating rate across the sample surface was less than 5%.

Surface temperatures were measured with a three-color recording pyrometer as discussed in reference 14. The pyrometer was focused directly onto the front surface of the sample. It was calibrated to account for absorption of radiation by the window in the door of the arc chamber and by the quartz dome on the sample chamber.

Test samples, conditions and procedures - The test samples were 0.64 cm diameter flat-faced cylinders. Heat fluxes ranged from about 29 MW/m^2 to 40 MW/m^2 as measured by the primary calorimeter. It will be shown later that the actual heat flux to the surface of the samples

was probably much less than measured. Test gases were air, nitrogen, helium and 90% CO_2 - 10% N_2, and the chamber pressure was varied from 0.3 to 8 atm.

The test samples were positioned in the holder with about 2/3 of the length extending out of the holder (Figure 3). The arc was initiated with the clam-shell shutter in the closed position, and the appropriate gas was injected into the sample chamber. When the desired operational conditions had been achieved the shutter was opened and the sample was exposed for five seconds. The shutter was then closed terminating the test. The outputs of the temperature pyrometer and the heat flux calorimeter were recorded continuously during each test.

Xenon-Arc Experiments

The tests in xenon-arc radiation were conducted in the xenon-lamp apparatus of the Entry Structures Facility at NASA's Langley Research Center. The apparatus consists of two xenon-arc units focused on a single area. A schematic diagram of the xenon-arc units and the test set-up is shown in Figure 6. The radiation is produced by a xenon arc and is collected and focused by an ellipsoidal mirror. After being focused by the mirror, the radiation passes through an optical integrator to produce a uniform beam. A lense system then refocuses the beam onto the sample area. The two lamp units are used to simultaneously irradiate the sample. The centerline of each unit makes an angle of about 50 degrees with the normal to the sample surface.

ORIGINAL PAGE IS
OF POOR QUALITY

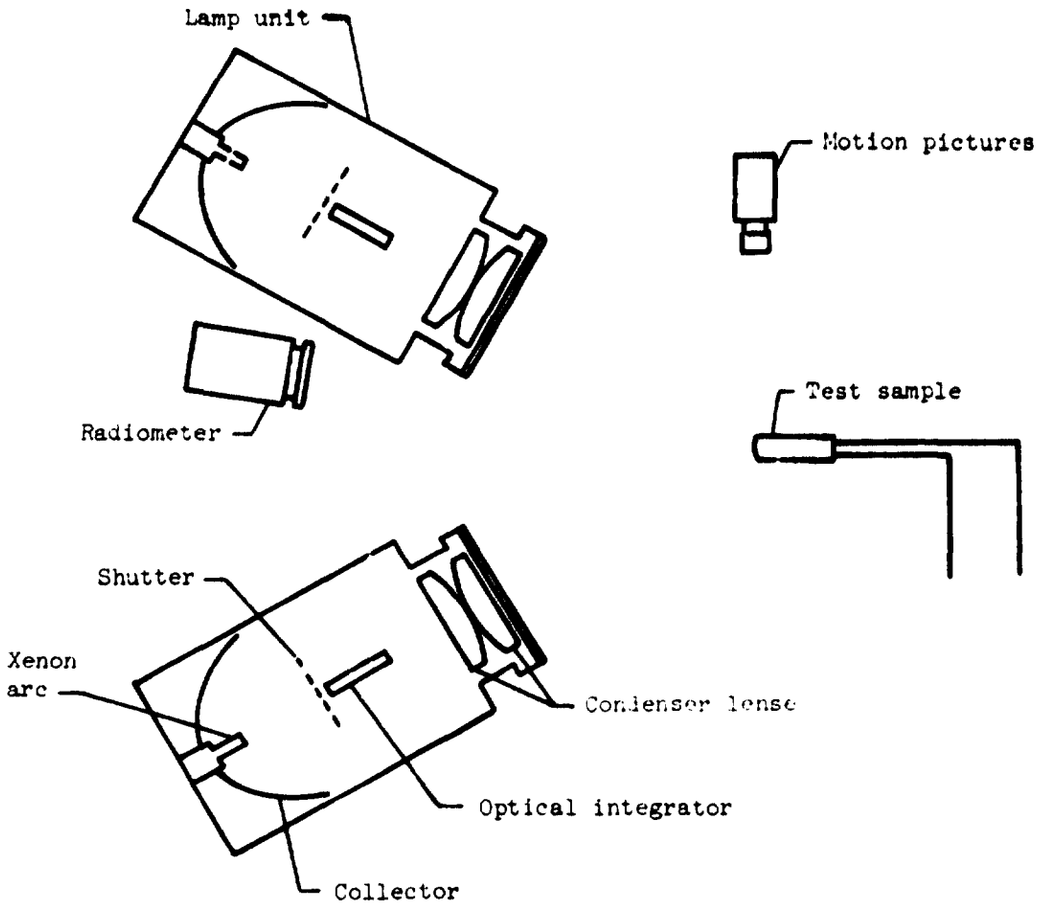

Figure 6.- Test set-up for xenon-arc experiments.

The samples were not enclosed in a test chamber. Hence, all tests were in air at one atm pressure. A fan was used to provide some air flow over the samples to remove the ablative products produced during the tests. A recording infrared radiometer was used to measure the surface temperatures. This instrument responds to radiation in the 8-16 μm wavelength range. Reflection of the arc-radiation from the sample surface should therefore not influence the temperature measurement.

The heat flux to the sample was measured by a water-cooled, black-body calorimeter. The heat flux measured by the calorimeter was correlated with the xenon-arc current which could be read directly from meters on the facility control panel. For each test the arc current was recorded as a measure of the incident heat flux. The calibration of the arc current in terms of the calorimeter was checked periodically. Heat fluxes in these tests were 10 MW/m^2 and 11.5 MW/m^2.

Test samples were 1.27 cm diameter cylinders with a blunted front surface. The test configuration is shown in Figure 3. This shape is the equilibrium shape for models exposed to the two xenon lamps positioned as shown in Figure 6. The shape was determined by exposing fluorogreen samples to the arc radiation for various times and examining the shape of the surface.

Tests were initiated and terminated with the electronically controlled shutters in each arc unit. The lamps were brought to the operating conditions with the shutters blocking the radiation. After the lamps had stabilized the shutters were opened, the sample exposed to the radiation for the required length of time, and the shutters closed, terminating the test.

ORIGINAL PAGE IS
OF POOR QUALITY

IV. ANALYSIS

Two different analytical programs were used to make theoretical predictions of the response of the materials to the heating environments; a one-dimensional charring ablator program, and a two dimensional subliming ablator program for the graphite. The basic equations and general features of the analyses required for the present study are given below. Details are given in references 6, 7, and 8.

Charring Ablator Program

The charring ablator program is a one-dimensional, numerical computer program which solves the governing equations for the transient response of thermal protection systems to heating environments. The program can treat a variety of systems but was developed primarily for charring ablators. The analysis is discussed in detail in reference 6. The essential features are discussed here. Three principle components are considered in the analysis; the uncharred ablator, a carbonaceous char layer resulting from the degradation of the ablator, and the pyrolysis gases generated when the ablator degrades upon heating (Figure 7). In general, the outer surface of the char and the interface between the char and the uncharred material are moving boundaries.

It is assumed that the thermal properties of a given layer are functions of temperature only, that all heat flow is normal to the heated surface, and that the pyrolysis gases are at the same temperature as the char. The governing equation within the char layer is:

ORIGINAL PAGE IS
OF POOR QUALITY

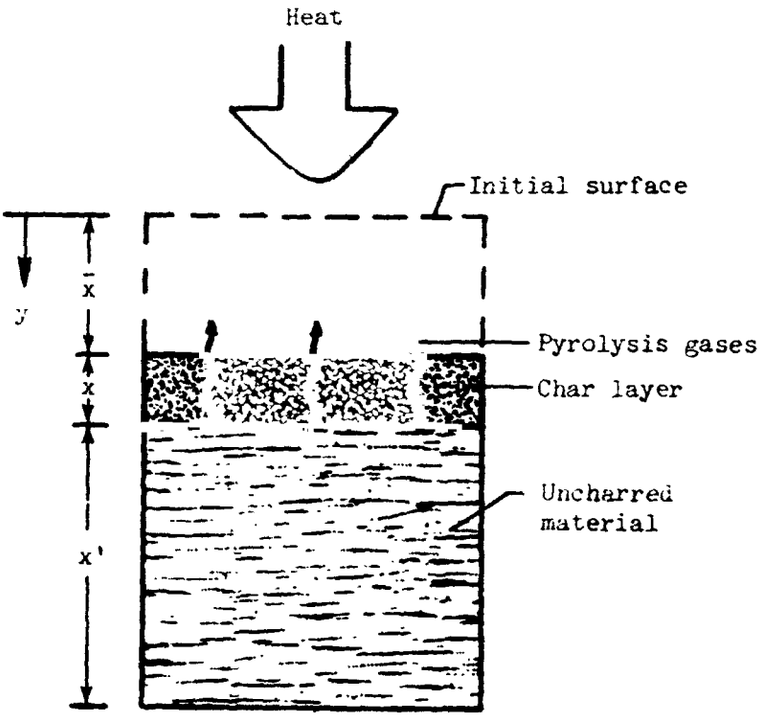

ORIGINAL PAGE IS
OF POOR QUALITY

Figure 7.- Charring ablator model used for one-dimensional calculations.

$$\frac{\partial}{\partial y}\left(k \frac{\partial T}{\partial y}\right) + \dot{m}_p \bar{c}_p \frac{\partial T}{\partial y} = \rho c_p \frac{\partial T}{\partial \tau} \tag{1}$$

The first term is the heat conducted, the second term is the heat absorbed by the transpiring gases, and the term on the right hand side of the equation is the heat stored. For the uncharred layer the governing equation is:

$$\frac{\partial}{\partial y}\left(k' \frac{\partial T'}{\partial y}\right) = \rho' c_p' \frac{\partial T'}{\partial \tau} \tag{2}$$

The initial temperature distribution must be given and is assumed to be a function of position:

$$T(y,0) = f(y) \tag{3}$$

Initial mass transfer rates must also be given and may or may not be zero. Two boundary conditions must be specified at the outer surface of the char. Either the rate of char removal or the surface temperature must be specified. The other condition is provided by a surface energy balance.

Surface material is considered to be removed by oxidation or sublimation. For sublimation, the char mass loss rate is related to the surface temperature by the expression:

$$\dot{m}_s = A_s e^{-B_s/T_w} \tag{4}$$

For a first-order oxidation reaction, the rate of char removal can be determined by the equation (reference 15):

$$\dot{m}_c = A_c(C_w P_w \zeta)\, e^{-B_c/T_w} \tag{5}$$

The rate at which char is oxidized is proportional to the rate at which oxygen diffuses to the surface (i.e. $\dot{m}_c = \lambda \dot{m}_{(O_2)}$). This rate is shown in reference 16 to be

$$\dot{m}_{(O_2)} = \frac{q_{c,net}}{h_e - h_w}(C_e - C_w) = \frac{\dot{m}_c}{\lambda} \tag{6}$$

where $q_{c,net}$ is the net convective heating rate to a hot ablating surface and is given by:

$$q_{c,net} = q_c\left(1 - \frac{h_w}{h_e}\right)\left\{1 - (1 - \beta)\left[0.6\,\frac{h_e}{q_c}(\alpha_c \dot{m}_c + \alpha_s \dot{m}_s) - 0.084\left(\frac{h_e}{q_c}\right)^2(\alpha_c \dot{m}_c + \alpha_s \dot{m}_s)^2\right] - \beta(\alpha_c \dot{m}_c + \alpha_s \dot{m}_s)\,\frac{h_e}{q_c}\right\} \tag{7}$$

The terms enclosed in the braces { } represent the reduction in heat transfer due to aerodynamic blocking by mass transfer. Either transpiration theory ($\beta = 0$) or linear ablation theory ($\beta = 1$) can be used to account for the effects of mass transfer on the convective heating rate. Combining equations (5) and (6) yields the expression for the rate of char removal by a first-order oxidation reaction:

$$\dot{m}_c = \frac{K P_w C_e \zeta}{1 + \frac{K P_w (h_c - h_w)\zeta}{\lambda q_{c,net}}} \tag{8}$$

where

$$K = A_c \, e^{-B_c/T_w}$$

Equation (4) or (8) can be used as the boundary condition for the rate of removal of the surface material. The surface energy balance is written as:

$$q_{net} = -k \frac{\partial T}{\partial y} \tag{9}$$

where the term on the right hand side represents conduction into the interior and

$$q_{net} = q_{c,net} + \alpha q_r + \dot{m}_c \Delta H_c - \dot{m}_s \Delta H_s - \sigma \varepsilon T_w^4 \tag{10}$$

① ② ③ ④ ⑤

The numbered terms in the above equation represent the following quantities:

1 convective heat input

2 radiative heat input

3 combustive heat input

4 heat absorbed by sublimation of char

5 heat reradiated from surface

The boundary condition at the interface between the char and the uncharred material is given by:

$$-k \frac{\partial T}{\partial y} = \dot{m}_p \Delta H_p - k' \frac{\partial T'}{\partial y} \tag{11}$$

The heat conducted to the interface must be either absorbed by pyrolysis reactions or conducted into the uncharred material. The pyrolysis rate is given by the expression

$$\dot{m}_p = A' e^{-B'/T} \tag{12}$$

where the reaction rate constant A' and the activation energy constant B' are determined experimentally by various thermoanalytical techniques (reference 17). For the present study, the back surface boundary condition allows for radiative exchange with a sink of known temperature, that is:

$$-k' \frac{\partial T'}{\partial y} = \sigma\varepsilon(T'^4 - T_b^4) \tag{13}$$

Subliming Ablator Program

For the graphite studies, a two-dimensional numerical analysis was used. This analysis treats the transient response of ablating, axisymmetric bodies including the effects of shape change. The analysis is described in detail in references (7) and (8) and only the salient features are given here. The system which can be analyzed is,

in general, a single orthotropic material of varying thickness with temperature dependent thermal properties. Figure 8 shows the general geometry used in the program. The particular geometries and numerical grid systems used for the present calculations are shown in Figure 9. For this investigation, the program was modified to account for the possibility of the absorption of radiation within the interior of the material instead of only at the surface. The governing time-dependent equation in fixed curvilinear coordinates is:

$$\frac{1}{h_1 h_2 h_3}\left[\frac{\partial}{\partial x}\left(\frac{h_2 h_3}{h_1} k_x \frac{\partial T}{\partial x}\right) + \frac{\partial}{\partial y}\left(\frac{h_1 h_3}{h_2} k_y \frac{\partial T}{\partial y}\right)\right] + \gamma q_r e^{-\gamma[\delta(x)-y]} = \rho C_p \frac{\partial T}{\partial \tau} \tag{14}$$

where h_1, h_2, h_3 are the scale factors for the coordinate system. A problem can be formulated in various coordinate systems by proper selection of the scale factors. The last term on the left in equation (14) accounts for the in-depth absorption of radiation. It is convenient to transform this equation to a moving coordinate system in which the finite difference stations remain fixed and the coordinates move to accommodate changes in surface location. The transformation is brought about by defining the quantities:

$$\xi = \frac{x}{x_b} \quad \text{and} \quad \eta = \frac{y}{\delta} \tag{15}$$

The transformed equation becomes:

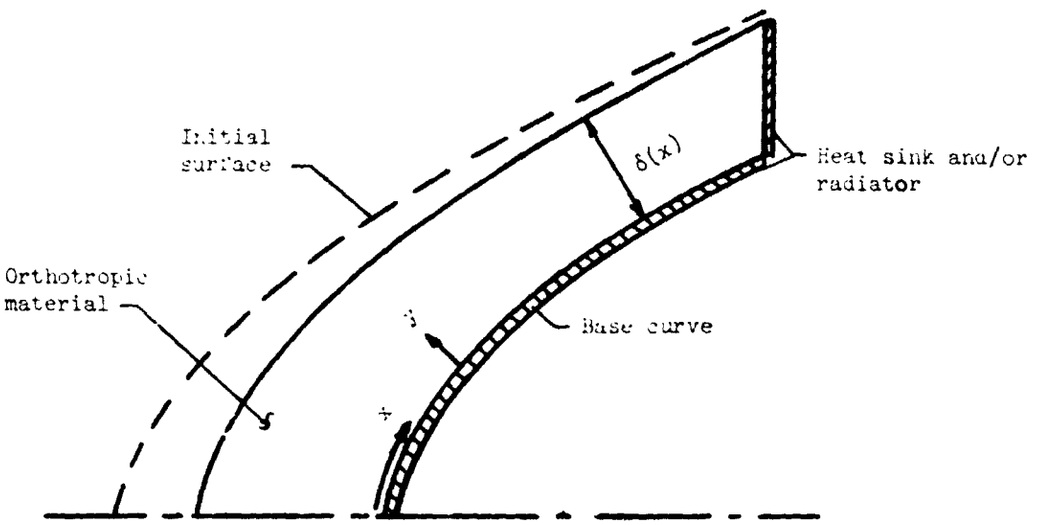

ORIGINAL PAGE IS
OF POOR QUALITY

Figure 8.- General subliming ablator geometry for two-dimensional calculations.

(a) Blunt model (xenon-arc samples)

(b) Flat model (laser and carbon-arc samples)

ORIGINAL PAGE IS
OF POOR QUALITY

Figure 9.- Numerical grid system for two-dimensional calculations.

$$\frac{1}{h_1 h_3}\left[\frac{1}{\delta^2}\frac{\partial}{\partial\eta}\left(h_1 h_3 k_\eta \frac{\partial T}{\partial\eta}\right) + \frac{1}{x_b^2}\frac{\partial}{\partial\xi}\left(\frac{h_3}{h_1} k_\xi \frac{\partial T}{\partial\xi}\right) - \frac{1}{x_b}\frac{\partial}{\partial\xi}\left(\frac{h_3}{h_1} k_\xi \eta \frac{A}{\delta}\frac{\partial T}{\partial\eta}\right)\right.$$

$$\left. - \frac{\eta A k_\xi}{\delta x_b}\frac{\partial}{\partial\eta}\left(\frac{h_3}{h_1}\frac{\partial T}{\partial\xi}\right) + \frac{\eta A}{\delta^2} k_\xi \frac{\partial}{\partial\eta}\left(\frac{h_3}{h_1}\eta A \frac{\partial T}{\partial\eta}\right)\right] + \gamma q_r e^{-\gamma\delta(1-\eta)}$$

$$= \rho c_p\left(\frac{\partial T}{\partial\tau} + \frac{\dot{m}}{\rho}\frac{\eta}{\delta}\frac{\partial T}{\partial\eta}\right) \tag{16}$$

where

$$A = \frac{1}{x_b}\frac{\partial\delta}{\partial\xi}$$

This is the general equation that is solved subject to various initial and boundary conditions. The initial conditions that must be specified are the temperature distribution, mass transfer rates, and the body shape. The front surface boundary conditions required are the same as for the charring ablator analysis discussed previously. Equations (5), (6), (7), and (8) for surface oxidation apply to the subliming analysis. The rate of ablation by sublimation is given by:

$$\dot{m}_s = \frac{A_s (P_w)^p e^{-B_s/T_w}}{(R_{stag})^r} \tag{17}$$

The surface energy balance in this case is

$$q_{net} = \frac{k_\eta}{\delta}\frac{\partial T}{\partial\eta} \tag{18}$$

where q_{net} is given by equation (10).

A number of boundary conditions may be specified along the back surface and edge of the body. These conditions include a constant property heat sink, radiation from these surfaces to e surface of a specified temperature, or any combination of these.

The heat input to the surface is affected by changes in body geometry as well as by aerodynamic blocking (equation (7)). The analysis adjusts the convective and radiative heat transfer rates to account for changes in body bluntness. The effects of geometry changes on the heating and pressure distributions around the body are also taken into account. Details are given in reference (7).

V. RESULTS AND DISCUSSION

Material performance is compared and evaluated on the basis of physical appearance, surface recession, and an ablative effectiveness parameter (reference 2) which is based on the depth of material degradation at the point of maximum heating. The effectiveness parameter is given by:

$$E = \frac{q_n t}{\rho \Delta \ell} \tag{18}$$

where q_n is the measured heat input (energy/unit time-unit area) less the heat reradiated at the point of maximum heating, t is the test time, ρ is the material density, and $\Delta \ell$ is the thickness of material degraded. The heat reradiated is computed from the maximum measured surface temperature. The emittance of the test materials in the charred state is taken as 0.9 (reference 18).

The results from all the tests in all facilities are summarized in Tables I and II. Table I gives the results of the charring ablator tests and Table II gives the graphite results.

Charring Ablator Experiments

Laser tests.- Figure 4 shows a typical heating distribution across the surface of a sample exposed to the laser radiation. This type of distribution is, in general, reflected in the shape of the sample surface after testing. The graphite samples are cupped slightly as expected, whereas the ablator chars (for those materials that developed

significant char) are almost completely hollowed out with only a thin shell of char remaining around the edge. These char shells are fragile and easily broken. Over most of the surface the interface between the char and the uncharred material was reasonably flat, indicating that the uncharred material was subjected to a fairly uniform heat flux. The sides of the material were apparently cooled sufficiently by radiation to allow a significant amount of char to build up. This behavior was typical of both high- and low- density phenolic nylon. Figure 10 is an oblique-view photograph of a typical high-density phenolic nylon sample after exposure to the laser environment. The hollow char shell is readily seen. The bubbles on the side are resolidified nylon that was melted by stray radiation inside the test chamber.

The epoxy material showed excessive surface recession with little or no char development. Any char that formed was quickly swept away. The carbon phenolic showed large amounts of cracking and spalling when exposed to the laser beam. Large chunks of material flew off, with considerable force, apparently because of thermal stresses built up within the material, and impinged upon the NaCl window in the front of the test chamber. The window thus began to heat up rapidly as it absorbed the laser radiation (resulting in large reductions in heat flux to the sample) and ultimately failed. Failure of the window occurred in times less than 0.5 sec. after initiation of the tests. Apparently the differences in thermal expansion characteristics of the phenolic resin, the carbon fibers, and the carbon formed by decomposition of the phenolic, coupled with the very rapid heating caused the failures of the carbon-phenolic materials.

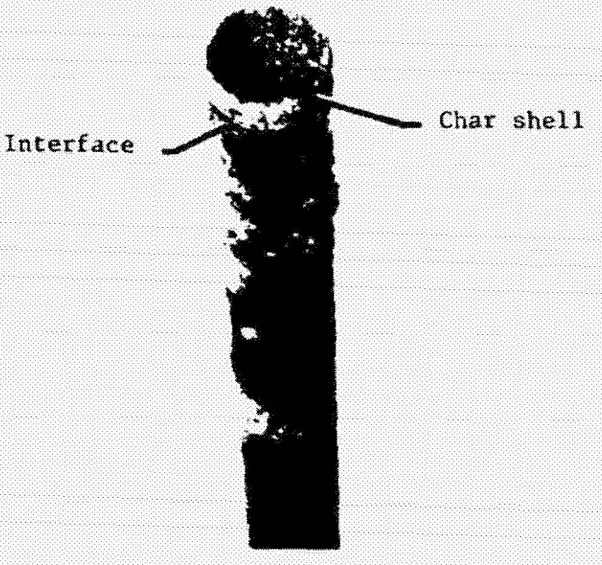

ORIGINAL PAGE IS
OF POOR QUALITY

Figure 10.- High density phenolic nylon after 2 second exposure to laser radiation at 42 MW/m^2 in air at 1 atm pressure.

The elastomer experienced a large surface recession as well as some bending and twisting during the tests. Its performance was comparable to that of the epoxy material. In the two environments in which it was tested, the PBI had the best performance of any of the charring ablators. A thick, relatively tough char layer developed over most of the front surface. It was however, subject to slight surface spallation. The appearance of each of the materials was about the same after testing in various environments.

The ablative effectiveness for phenolic-nylon and the PBI is shown in Figure 11. Effectiveness values were computed with equation 18 and then normalized with respect to the value for LDPN in air at 1 atm. pressure. The PBI was tested in only two environments but performed better than the other ablators in these environments. The LDPN performed better than the HDPN in all tests but the differences in effectiveness were in general not large. Neither chamber pressure nor test gas had a large effect on the performance of the materials. The materials performed about the same in air as in nitrogen and helium. This behavior is likely caused by the large quantity of gases generated by the degradation of the material limiting the amount of test gas reaching the degrading surface.

Effectiveness values for the phenolic-carbon could not be determined because of the severe spallation. The very rapid recession and irregular surfaces of the epoxy and the elastomeric materials made surface temperature and recession measurements questionable at best and no effectiveness values are given. However, if a temperature equal

ORIGINAL PAGE IS
OF POOR QUALITY

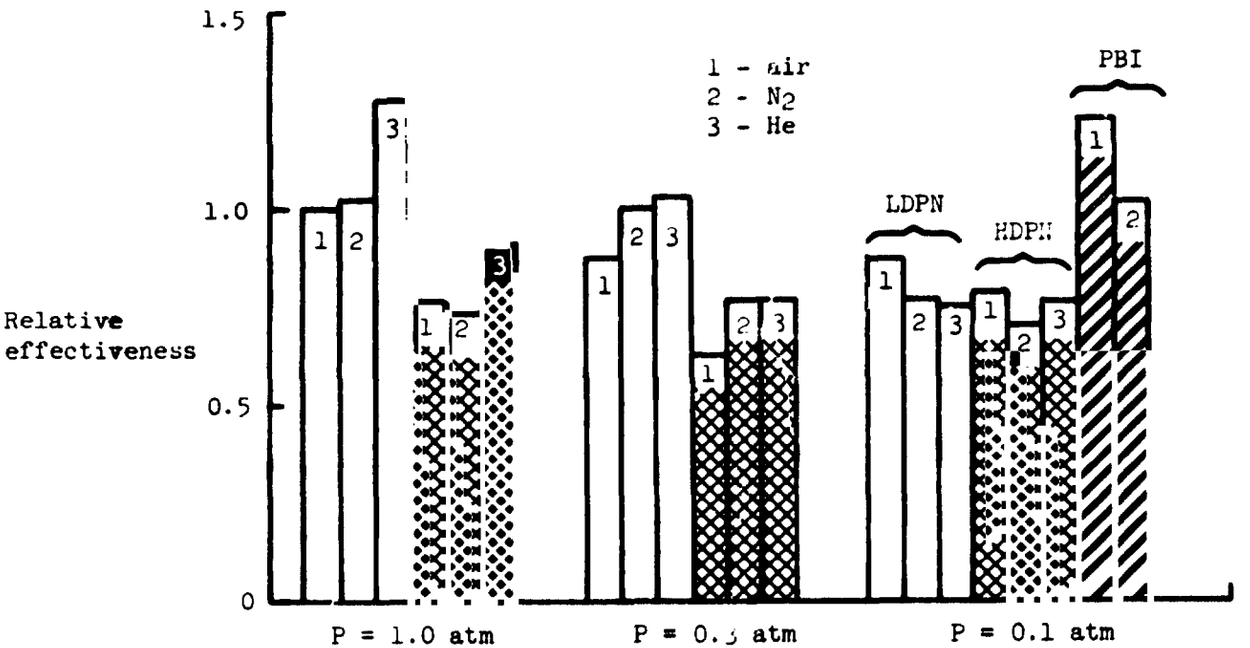

Figure 11.- Relative effectiveness of charring materials in laser environments.

to the sublimation temperature of graphite at the given pressure is assumed (references 19 and 20), and an average recession is used, the effectiveness of these two materials is about half that of LDPN.

Carbon-arc tests.- The materials that were tested in both the laser and the carbon arc (graphite, LDPN, and epoxy) appeared to perform much better in the carbon arc at what was supposed to be approximately the same test conditions. The mass lost and surface recessions were much smaller and the effectiveness values were much greater in the carbon-arc tests (see tables 1 and 2). However it is probable that the actual heat fluxes to the samples in the carbon arc were significantly less than those measured because of the absorption of incoming radiation by the ablative gases. The sample chamber and gas flow arrangement (Figures 3 and 5) is such that the ablative gases were not swept away cleanly and a significant volume of gas was built up in front of the sample. Figure 12 shows the spectral absorption coefficient for a carbon plasma at 3000 K and 1 atm. pressure (from reference 21). For comparison, the spectral energy distribution of the carbon arc is superimposed on the absorption coefficient curve. It is seen that over almost the entire spectral range of the carbon-arc radiation, the absorption coefficient is significant, approaching 100 cm^{-1}. The heat flux to the sample thus could be reduced substantially by the absorption of arc radiation by the ablative gases. For example, if an absorption coefficient of only 1 cm^{-1} is used, and it is assumed that there is the equivalent of just 1 cm of gas through which the radiation must pass to reach the surface, the heat flux is reduced by almost two-thirds

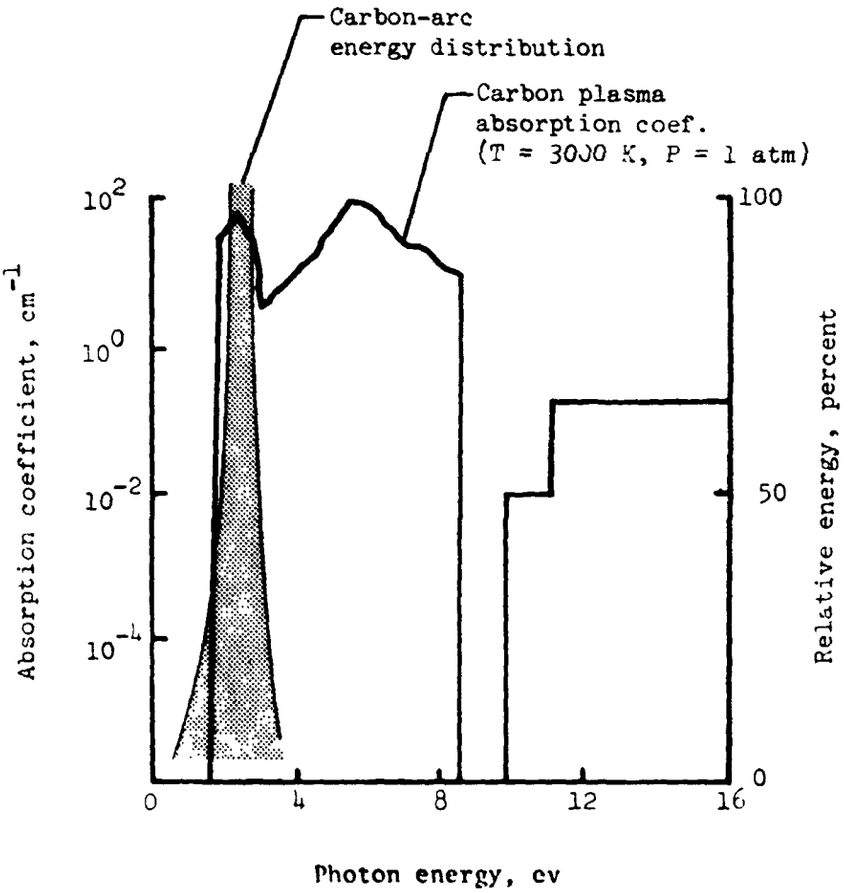

ORIGINAL PAGE IS
OF POOR QUALITY

Figure 12.- Spectral distributions of carbon-plasma absorption coefficient and carbon-arc energy output.

of the incoming value. The average effectiveness for LDPN in the carbon arc is about 85 MW/m^2, based on the measured heat flux, and only about 23 MW/m^2 based on a corrected heat flux (table 1). This lower value agrees very well with those for LDPN in the laser tests. In determining a corrected heat flux, it is assumed that there is one centimeter of ablative gases with an absorption coefficient of 1 cm^{-1} in front of the sample. In light of figure 12 and the geometry of the test set-up, these assumptions appear to be reasonable.

Figure 13 gives the relative effectiveness (corrected heat flux) for the ablators tested in the carbon arc. The dashed lines on the figure show the band within which the effectiveness values for the laser tests fall. The LDPN and the P-3 material performed best with effectiveness values in the range of those for the laser tests. The P-1 and P-2 had greater interface recession in spite of their higher densities and hence had low effectiveness. Again the elastomer and the Apollo material had relatively large recession rates. As expected, the materials performed somewhat better in inert atmospheres than in air. However, the differences in performances were not large. There was little difference in the material behavior in air and in the CO_2 - N_2 atmosphere. Again there was no apparent effect of pressure over the range considered.

Figure 14 shows photographs of the materials tested in the carbon arc in air at 1 atm. pressure. The LDPN, P-2, and P-3 materials developed relatively thick chars over the surface and showed little or no front surface recession around the edge. The surfaces were cupped

ORIGINAL PAGE IS OF POOR QUALITY

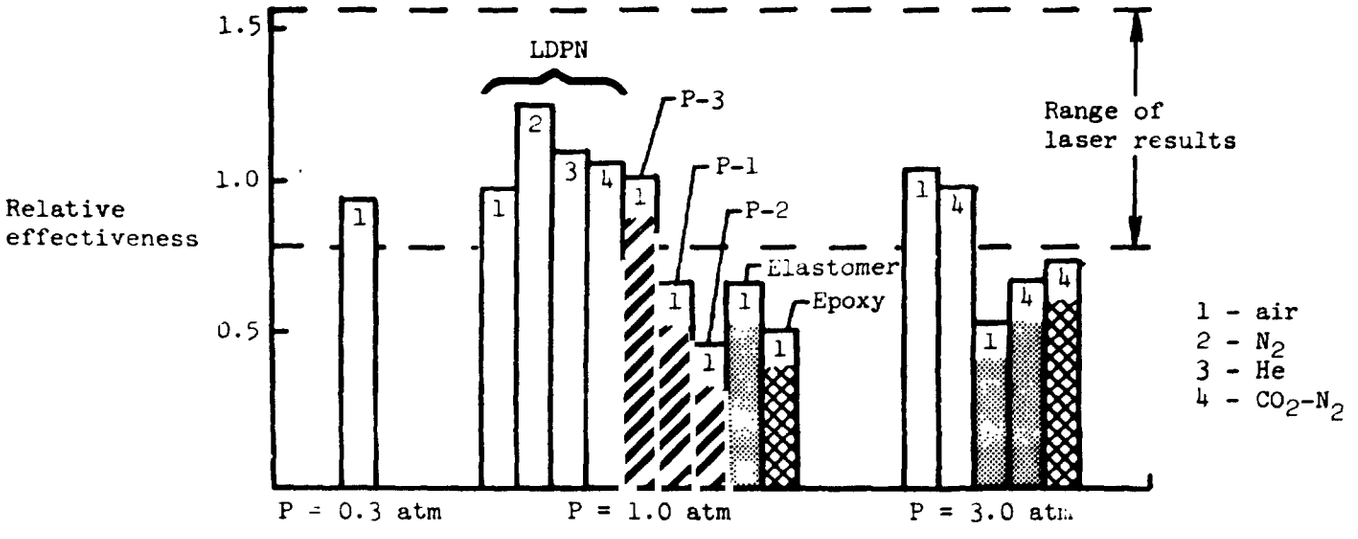

Figure 13.- Relative effectiveness of charring ablators in carbon-arc environments (corrected heat flux).

ORIGINAL PAGE IS
OF POOR QUALITY

Material	Graphite	LDPN	P-1	P-2	P-3	Epoxy	Elastomer
Heat flux MW/m^2	15.6	14.8	11.8	12.3	12.8	12.3	12.3

Figure 14.- Test samples after 5 second exposure to carbon-arc radiation in air at 1 atm pressure.

slightly because of the radiative cooling around the sides. The interface between the char and the uncharred material was weak and the char tended to separate from the sample. This behavior is also typical of these materials in low heat-flux convective environments.

The P-1 material had a very thin (< 1 mm) fully developed char and a somewhat larger depth of partially degraded material. The char was tough and strongly attached. Although the effectiveness of P-1 was rather low, the physical appearance and surface integrity were better than those of the other ablators.

Figure 15 shows the LDPN after testing in the various gases at one atmosphere pressure. There is no significant difference in the physical appearance of the samples. In general the CO_2 - N_2 atmosphere appeared to produce the greatest front surface recession. The interface recessions were about the same in air and in CO_2 - N_2, but the CO_2 - N_2 sample had a noticeably thinner char. This is most likely due simply to the greater oxygen concentration in the CO_2 - N_2 gas mixture resulting in increased oxidation.

To determine whether or not there was some microscopic differences in the chars developed, scanning electron microscope (SEM) photographs were made of the LDPN chars. Figure 16 shows the front surface of the chars after testing in the various environments. Comparison of the photographs showed no significant differences in the appearance or structure of any of the chars. Also there is no evidence of any carbon deposition within the char as has been observed in some low heat-flux convective environments. Apparently the material responded fundamentally the same in all environments.

ORIGINAL PAGE IS
OF POOR QUALITY

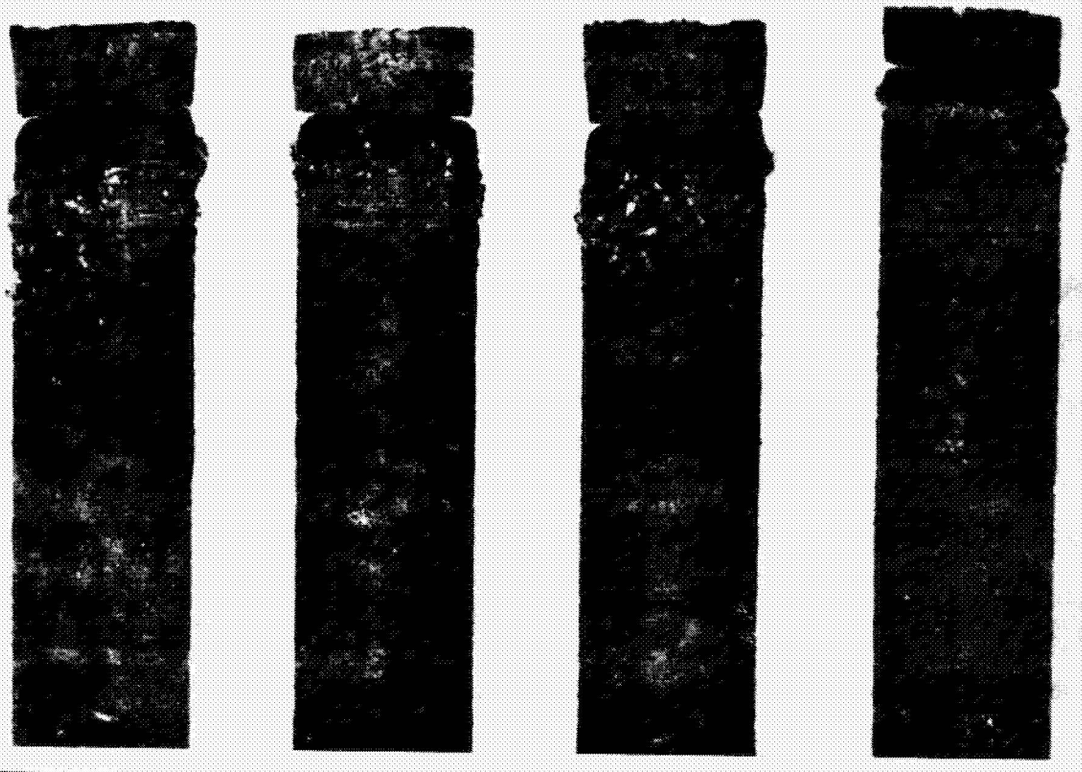

Test gas	Air	Nitrogen	Helium	90% CO_2 - 10% N_2
Heat flux MW/m^2	14.8	14.4	13.9	11.8

Figure 15.- Low density phenolic nylon after 5 second exposure to carbon-arc environments at 1 atm. pressure.

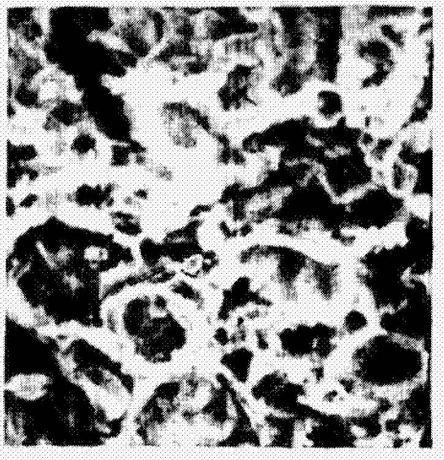

Air

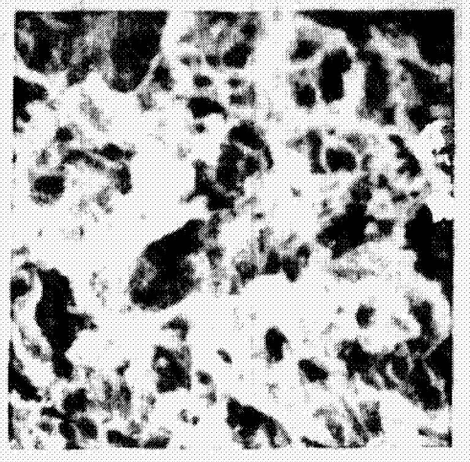

Nitrogen

Helium

90% CO_2 - 10% N_2

Figure 16.- Scanning electron photomicrographs of low-density phenolic nylon char after exposure to carbon-arc environments at 1 atm. pressure (200X).

ORIGINAL PAGE IS
OF POOR QUALITY

Graphite Experiments

Table II gives a summary of all the graphite test results. Material performance is evaluated on the basis of mass loss rates and/or surface recessions. There was no measureable surface recession in the carbon-arc tests.

Mass loss rate data for the various laser environments are given in Figure 17. The rates are based on surface recession at the center of the sample front surface. There is no significant difference in the performance in nitrogen and in helium. Also there is no apparent effect of pressure on material performance over the range considered (0.1 - 1.0 atm.). As expected, mass loss rates are greater in air than in the other gases.

Mass loss rates for graphite in the carbon-arc environments are shown in Figure 18. Since there was no measureable recession in these tests, the mass loss rates are based on sample weights before and after testing. The symbols indicate the average values and the bars show the data scatter. The scatter is due primarily to variations in incident heat flux. In general the mass loss rates for the carbon-arc test were much less than those in the laser tests, even though the measured heat fluxes were comparable. Again it is probable that, in the carbon-arc tests, the actual heat fluxes to the samples were significantly less than the measured values, primarily because the test configuration allowed a considerable volume of test gas and ablative products to build up in front of the samples. The results are more consistent if a corrected heat-flux is considered as discussed previously under the

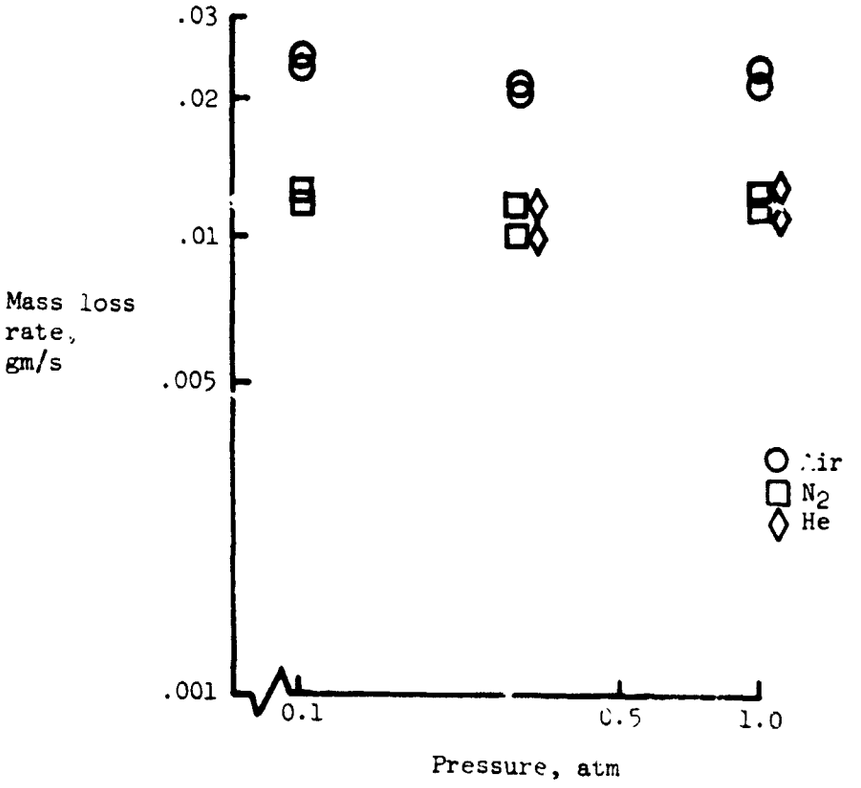

ORIGINAL PAGE IS OF POOR QUALITY

Figure 17.- Experimental mass loss rates for graphite in laser tests.

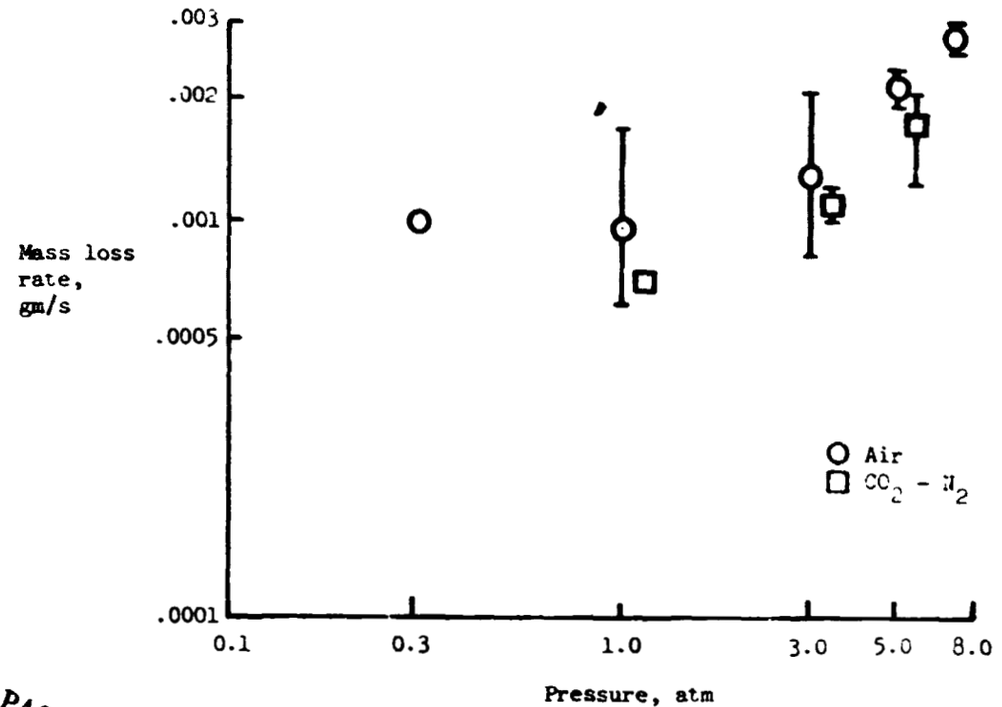

ORIGINAL PAGE IS OF POOR QUALITY

Figure 18.- Experimental mass loss rates for graphite in carbon-arc tests.

charring ablator carbon-arc tests. The results then also agree reasonably well with those of reference 22 as well as with the analytical results to be discussed later.

There is little difference in the graphite behavior in air and in the CO_2 - N_2 gas mixture. In each gas there is a trend for the mass loss rate to increase with increasing pressure from 1 to 3 atm. In the present studies, this effect appears to be a result of the graphite microstructure as well as thermochemical phenomena, although reference 23 reports a correlation in which the mass loss rate is directly proportional to the pressure. If, at the higher pressures, larger molecules are being removed from the surface, the heat of sublimation is reduced and there is a corresponding increase in the mass loss rate. Also, graphite microstructure is nonhomogenous and can vary significantly. It is shown in reference 24 that grain size and porosity, in particular, have a major influence on graphite ablative performance. For the present tests, photomicrographs of graphite (Figure 19) show that the samples tested at the higher pressures have significantly larger grain size and greater porosity. This large grain size and open porosity allow greater subsurface oxidation and possibly in-depth removal of binder material and hence resulted in greater mass loss. Photomicrographs of graphite tested in CO_2 - N_2 show the same trend.

Analytical Results

Calculations were made only for the graphite and the phenolic nylon because these materials are well characterized and their thermophysical properties are best known. Also, the analyses used can not treat

P = 1 atm

P = 3 atm

P = 5atm

Figure 19.- Scanning electron photomicrographs of graphite after testing in carbon arc in air (1000X).

ORIGINAL PAGE IS
OF POOR QUALITY

mechanical removal of material such as occurred with several of the materials tested. The thermophysical properties of phenolic nylon were obtained from reference 10, and those of graphite from reference 25. The sublimation parameters were obtained from reference 22 (ΔH_s) and reference 26 (A_s and B_s in equation 17). The analysis of reference 26 is a simplified chemical-nonequilibrium treatment of charring ablator and graphite sublimation and yields results which are in good agreement with the experimental results of reference 23.

Figure 20 shows the experimental and calculated results for one graphite test in the laser facility in air, at 1 atm pressure, at a heat flux of 45.8 MW/m^2. The calculated surface recession at the end of a 5 second test is compared with the measured values. The scale on the ordinate is inverted so that the curves shown indicate the actual shape of the front surface from the sample centerline ($s/R = 0$) to the sample edge ($s/R = 1$). The dashed line shows the original shape of the sample. The agreement between the calculated and experimental results is, in general, reasonably good. Although there is some difference in the results at the sample centerline, the magnitude of this difference is only about 0.5 mm. Attempts to lessen the difference by invoking mass loss mechanism other than sublimation and oxidation were unsuccessful. Absorption of radiation below the front surface with subsequent periodic explosive mass removal could lead to increases in recession, as could preferential ablation of the graphite binder. However, in the present graphite tests, no significant particulate removal was observed. Phenomena such as electric field effects

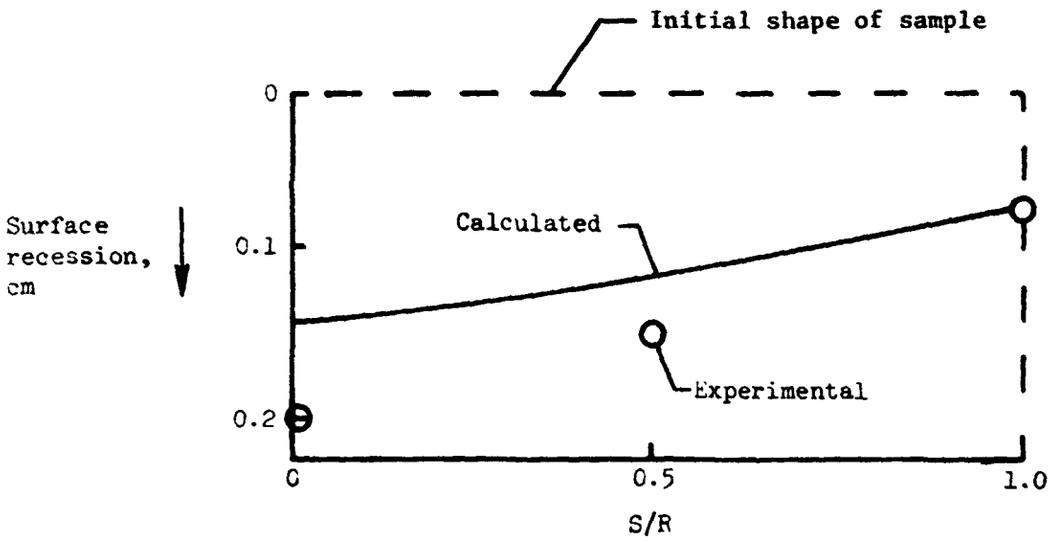

ORIGINAL PAGE IS OF POOR QUALITY

Figure 20.- Experimental and calculated graphite recession in laser facility - air, 1 atm, 45.8 MW/m^2.

associated with intense laser beams, direct interaction of photons with atoms and molecules to dissociate carbon-carbon bonds, multi-photon effects, and others are possible contributors to additional mass loss (reference 27). They are, however, unusual effects and simple analysis indicates that the associated mass loss rates are negligible compared to those observed. Some typical results for graphite tests in nitrogen and helium atmospheres in the laser facility are shown in Figures 21 and 22. In these cases, the agreement between the calculated and experimental results is very good.

Figure 23 shows typical results for graphite tests in the carbon-arc facility. Two sets of calculations are compared with the experimental results. The calculations in which the measured heat flux was used predict large recession rates whereas the tests showed no measurable recession. However, if the corrected heat flux is used, the calculations show negligible recession, in agreement with the experiment. Similar results were obtained for all other environments in the carbon-arc tests.

Further evidence that the heat flux to the ablating samples in the carbon arc was much less than that measured in the absence of ablation is given by the phenolic nylon results shown in Table 3 and in Figures 24, 25 and 26. Time histories of the stagnation point surface and interface recessions are given for both the measured and the corrected heat flux for tests in air at various pressures. Both the surface and interface recessions calculated with the corrected heat flux are seen to agree very well with the measured values. These

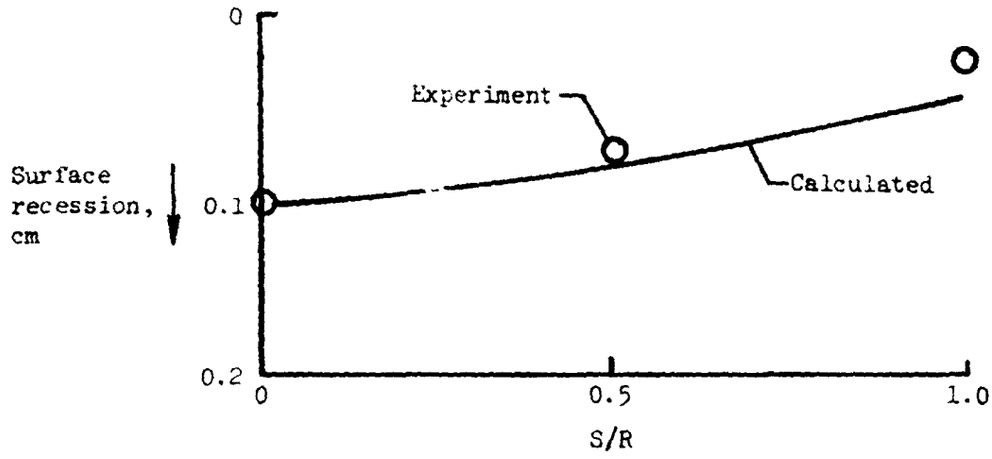

ORIGINAL PAGE IS
OF POOR QUALITY

Figure 21.- Experimental and calculated graphite recession in laser facility - nitrogen, 1 atm, 40.8 MW/m^2.

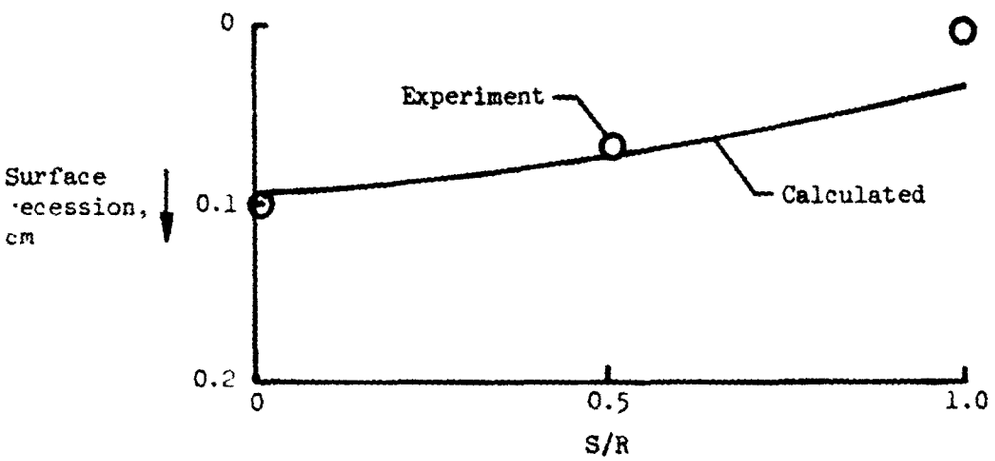

ORIGINAL PAGE IS
OF POOR QUALITY

Figure 22.- Experimental and calculated graphite recession in laser facility - helium, 1 atm, 38.0 MW/m^2.

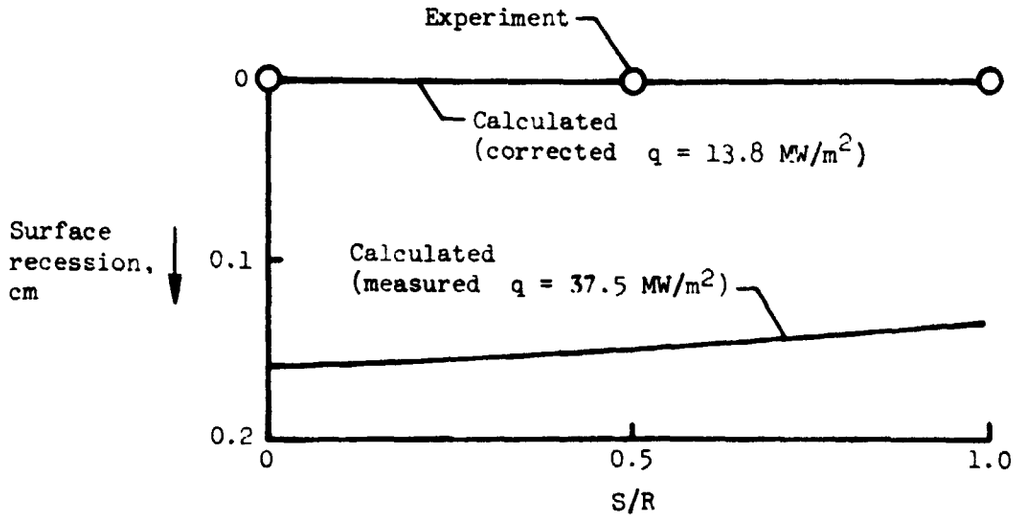

ORIGINAL
OF POOR QUALITY

Figure 23.- Experimental and calculated graphite recession in carbon arc facility - air, 1 atm.

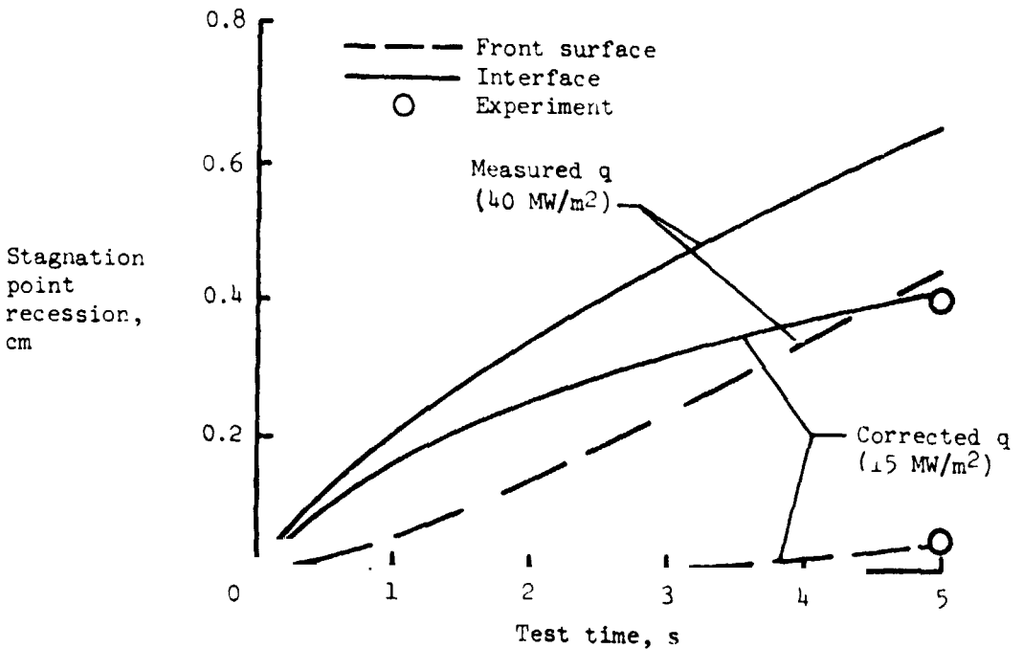

ORIGINAL PAGE IS
OF POOR QUALITY

Figure 24.- Experimental and calculated recessions for low-density phenolic nylon in carbon-arc facility-air, 1 atm.

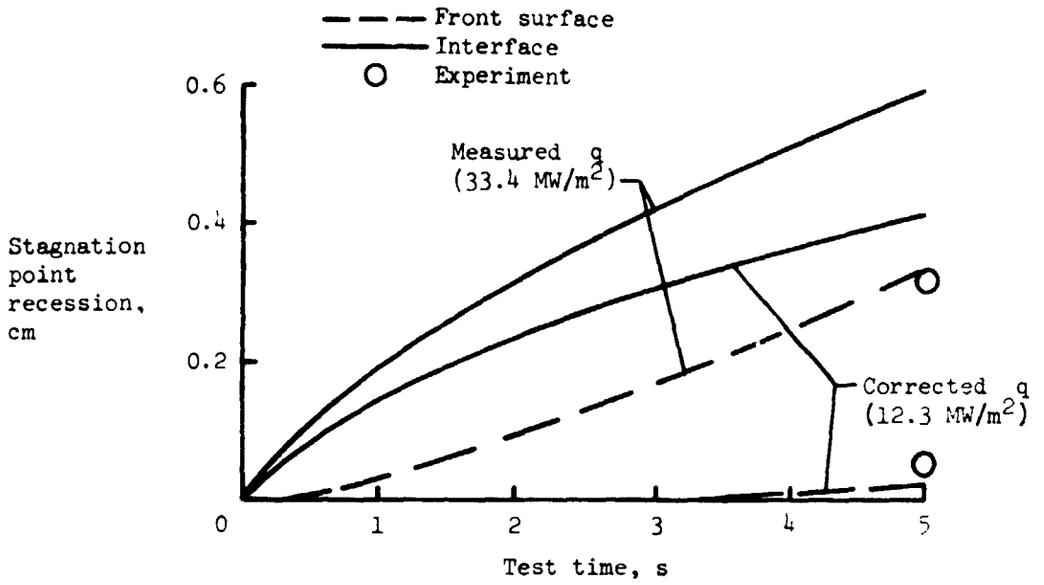

Figure 25.- Experimental and calculated recessions for low-density phenolic nylon in carbon-arc facility-air, 0.3 atm.

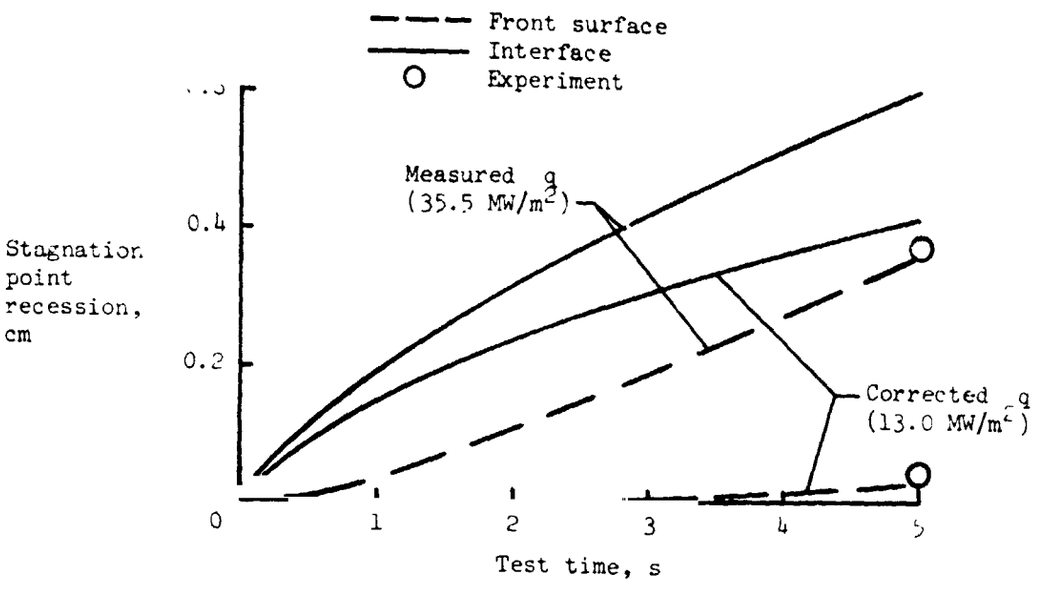

Figure 26.- Experimental and calculated recessions for low-density phenolic nylon in carbon-arc facility-air, 3.0 atm.

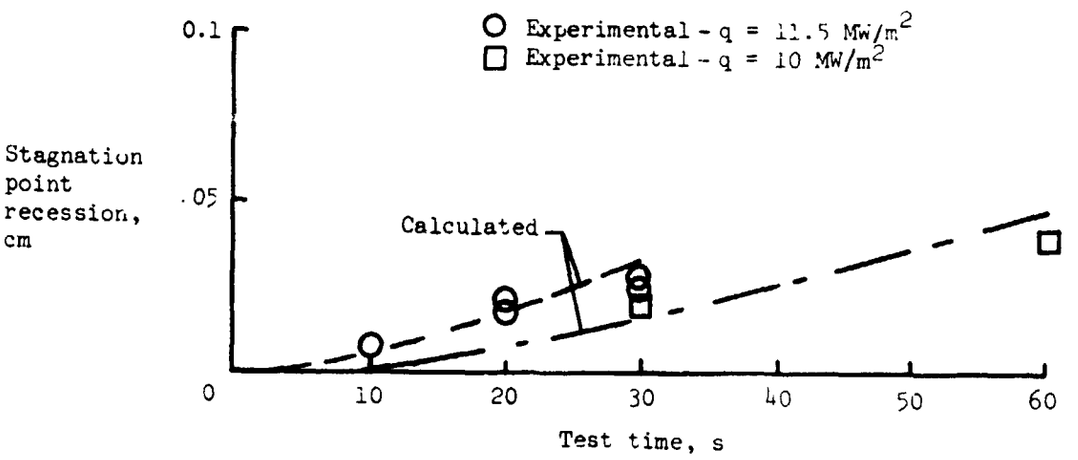

Figure 27.- Experimental and calculated graphite recession in xenon-arc facility-air, 1 atm.

calculations were made with the one-dimensional charring ablator analysis.

Results for the xenon-arc experiments and calculations for graphite are given in Figure 27. Time histories of the stagnation point surface recession are shown for two heat fluxes. Again the two-dimensional sublimation analysis satisfactorily predicts the material response.

In the tests discussed here, no attempt was made to simulate all aspects of actual planetary entry environments. At present, there are no ground test facilities capable of such simulation. The present results do give an indication of how a given material will react to radiative heat fluxes of the level associated with high velocity planetary entry. The results also show how the performance of a material may be affected by the different types of atmospheric gases that a spacecraft may encounter (for example, air for Earth entry and CO_2-N_2 for Venus entry). These factors are important when making an assessment of what types of materials may be candidates for thermal protection systems in actual reentry situations. The results also give confidence in the ability to predict material behavior given appropriate material and enviornmental inputs. Differences in test and flight environments will, of course, have to be taken into account when extrapolating these predictions to actual reentries.

VI. CONCLUDING REMARKS

Results are presented from an investigation of the behavior of graphite and several charring ablators in various high radiative heat flux environments. A commercial grade graphite and six state-of-the-art charring ablators were subjected to radiative heating environments produced by a CO_2 laser, a carbon arc, and a xenon arc. Heat flux levels ranged from 10 to 47 MW/m^2. The experimental results are compared to theoretical calculations.

Scanning electron microscopy showed no significant differences in appearance, composition, or microstructure of the charring ablators or graphite after testing in the three different radiative facilities. Apparently the materials responded fundamentally the same to the radiation of different frequencies.

The performance of phenolic nylon and graphite in the radiative environments can be satisfactorily predicted with existing analyses and published sublimation data. Good agreement between experimental and analytical results is obtained with constants from a simplified chemical non-equilibrium analysis of graphite sublimation.

There are state-of-the-art charring ablators that can satisfactorily withstand radiative fluxes typical of those encountered in Venus entry. The low-density phenolic nylon and PBI performed well. The epoxy material (Apollo heat shield material) and the silicone elastomer showed excessive surface recession in all test conditions and appear to be unsuitable for the severe radiative environments. When exposed to

the laser radiation, the carbon-phenolic showed large amounts of cracking and spalling apparently because of differential thermal expansion between the phenolic resin and the carbon fibers. It is significant that some of the lower density materials showed the best performance because the low density would mean reduced heat shield weight for an entry vehicle.

In the laser tests, the charring ablators behaved about the same in air, nitrogen, and helium atmospheres. In the carbon arc, the materials performed slightly better in nitrogen and helium than in air, but the differences in performance were small. The 90% CO_2 - 10% N_2 atmosphere produced about the same interface recession in phenolic nylon as did air but resulted in slightly greater char loss. Variations in chamber pressure over the range 0.1 - 3.0 atm had no significant effect on the performance of the charring ablators.

There was no significant difference in the behavior of graphite in nitrogen and helium in either of the facilities, but the mass loss rates were somewhat greater in air and in 90% CO_2 - 10% N_2. There was also little difference in the graphite performance in air and in CO_2 - N_2. Variation in pressure from 0.1 to 1.0 atm did not effect the performance of graphite whereas there was a trend of increasing mass loss rate with increasing pressure from 1.0 to 8.0 atm. This trend was seen in both air and in CO_2 - N_2.

REFERENCES

1. Dow, Marvin B.; and Brewer, William D.: Performance of Several Ablation Materials Exposed to Low Convective Heating Rate in an Arc-jet Stream. NASA TN D-2577, June 1965.

2. Swann, Robert T.; Brewer, William D.; and Clark, Ronald K.: Effect of Composition, Density, and Environment on the Ablative Performance of Phenolic Nylon. NASA TN D-3908, April 1967.

3. Tompkins, Stephen S.; and Kabana, Walter P.: Effects of Material Composition on the Ablation Performance of Low-Density Elastomeric Ablators. NASA TN D-7246, May 1973.

4. Meyer, Carl B.; and Rindal, Ronald A.: An Analysis of the Coupled Chemically Reacting Boundary Layer and Charring Ablator. NASA CR-1061, June 1968.

5. Scala, Sinclaire M.; and Gilbert, Leon M.: Thermal Degradation of a Char-Forming Plastic During Hypersonic Flight. ARS Jour., vol. 32, no. 6, June 1962, pp. 917-924.

6. Swann, Robert T.; Pittman, Claud M.; and Smith, James C.: One-Dimensional Numerical Analysis of the Transient Response of Thermal Protection Systems. NASA TN D-2976, 1965.

7. Tompkins, Stephen S.; Moss, James N.; Pittman, Claud M.; and Howser, Lona M.: Numerical Analysis of the Transient Response of Ablating Axisymmetric Bodies Including the Effects of Shape Change. NASA TN D-6220, 1971.

8. Howser, Lona M.; and Tompkins, Stephen S.: Computer Program for Transient Response of Ablating Axisymmetric Bodies Including the Effects of Shape Change. NASA TM X-2375, 1971.

9. Scala, S. M.; and Gilbert, L. M.: Sublimation of Graphite at Hypersonic Speeds. AIAA Jour. vol. 3, no. 9, Sept. 1965.

10. Wilson, R. G.: Thermophysical Properties of Six Charring Ablators from 140°K to 700°K and Two Chars from 800°K to 3000°K, NASA TN D-2991, 1965.

11. Dickey, R. R.; Lundell, J. H.; and Parker, J. A.: Development of Polybenzimidazole Composites as Ablative Heat Shields. Journal of Macromolecular Science-Chemistry, vol. A3, no. 4, July 1969, pp. 573-584.

12. Horrigan, F. A.; Klein, C. A.; Rudko, R. I.; and Wilson, D. T.: High Power Gas Laser Research. Final Technical Report Contract No. OA-AH01 67-1589, September 1968. Raytheon Research Division, Waltham, Mass.

13. Baker, E. Jack, Jr.: Thermal Radiation Testing of Ablative Heat Protective Materials with an Arc-Image Furnace. Final Report, Contract No. NAS9-3416, 1965.

14. Baker, E. Jack, Jr.: Determination of Surface Temperature and Emissivity. Final Report, Project 02-1862, Southwest Research Institute, 1966.

15. Nolan, Edward J.; and Scala, Sinclaire M.: Aerothermodynamic Behavior of Pyrolytic Graphite During Sustained Hypersonic Flight. ARS Journal, vol. 32, no. 1, Jan. 1962, pp. 26-35.

16. Swann, Robert T.: Approximate Analysis of the Performance of Char-Forming Ablators. NASA TR R-195, 1964.

17. Nelson, James B.: Determination of Kinetic Parameters of Six Ablation Polymers by Thermogravimetric Analysis. NASA TN D-3919, 1967.

18. Wilson, R. Gale: Hemispherical Spectral Emittance of Ablation Chars, carbon, and Zirconia to 3700 K. NASA TN D-2407, 1965.

19. Glockler, G.: Journal Chem. Phys., vol. 22, p. 159 (1954).

20. Zavitsanos, P. O.: Mass Spectrometric Analysis of Carbon Species Generated by Laser Evaporation. Carbon 1968, vol. 6, pp. 731-737.

21. Nelson, H. F.: Radiative Transfer Through Carbon Ablation Layers. Jour. of Quantitative Spectroscopy and Radiative Transfer. Vol. 13, pp. 427-445, 1973.

22. Davy, W. C.; and Bar-Nun, Akiva: Vaporization Characteristics of Carbon Heat Shields Under Radiative Heating. AIAA Paper no. 72-296, San Antonio, TX., April 10-12, 1972.

23. Bishop, W. M.; and DiCristina, V.: The Combustion and Sublimation of Carbon at Elevated Temperatures. AIAA Paper no. 68-759, Los Angeles, CA, June 24-26, 1968.

24. McVey, D. F.; Auerbach, I.; and McBride, D. D.: Some Observations on the Influence of Graphite Microstructure on Ablation Performance. AIAA paper no. 70-155, NY, NY, Jan. 19-21, 1970.

25. Wakefield, Roy M.; and Peterson, David L.: Graphite Ablation in Combined Convective and Radiative Heating. Journal of Spacecraft and Rockets, vol. 10, no. 2, Feb. 1973, pp. 149-154.

26. Balhoff, John F.; and Pike, Ralph W.: Modeling Sublimation of a Charring Ablator. Journal of Spacecraft and Rockets, vol. 10, no. 12, Dec. 1973, pp. 822-824.

27. Ensign, Thomas C.; and Lye, Robert C.: Effects of Intense Ultraviolet Radiation on Carbonaceous Ablative Heat Shields. RIAS Technical Report 71-23, Oct. 1971, Research Institute for Advanced Studies, Martin Marietta Corp., Baltimore, Md.

Table 1.- Charring Ablator Test Results

Facility	Material	Test gas	Pressure, atm	Heat flux, MW/m^2		Surface temperature, K	Test time, s	Δx, cm	$\Delta \ell$, cm	Δm, gm	E, MJ/kg	E^c, MJ/kg
				Measured	Corrected							
Laser	LDPN	Air	0.1	42.0	-	3130	2	-	.560	.164	24.1	-
			0.3	42.0	-	3520		-	.510	.145	24.4	-
			1.0	42.6	-	3350		-	.460	.162	28.6	-
		N_2	0.1	40.5	-	3520		-	.560	.170	21.2	-
			0.3	41.1	-	3280		-	.460	.122	27.8	-
			1.0	40.6	-	3390		-	.430	.140	28.6	-
		He	0.1	41.0	-	3660		-	.560	.162	20.7	-
			0.3	36.5	-	3180		-	.406	.113	28.0	-
			1.0	45.9	-	3290		-	.406	.103	35.8	-
	HDPN	Air	0.1	42.0	-	2940	2	-	.305	.127	21.8	-
			0.3	42.0	-	3580		-	.330	.209	17.7	-
			1.0	42.0	-	3300		-	.330	.210	19.0	-
			1.0	43.5	-	3280		-	.305	.126	21.4	-
		N_2	0.1	41.8	-	3520		-	.305	.123	19.4	-
			0.3	41.9	-	3110		-	.305	.092	21.2	-
			1.0	40.7	-	3450		-	.280	.099	20.8	-
		He	0.1	41.0	-	3660		-	.254	.116	21.8	-
			0.3	36.1	-	3180		-	.254	.082	21.1	-
			1.0	43.3	-	3300		-	.254	.084	25.5	-

Table 1.- Continued.

Facility	Material	Test gas	Pressure, atm	Heat flux, MW/m^2		Surface temperature, K	Test time, s	Δx, cm	$\Delta \ell$, cm	Δm, gm	E, MJ/kg	E^c, MJ/kg
				Measured	Corrected							
Laser	PC	Air	0.1	43.0	-	-	2	-	-	.103	-	-
			0.3	41.0	-	-		-	-	.088	-	-
			0.3	42.5	-	-		-	-	.098	-	-
			1.0	42.0	-	-		-	-	.135	-	-
			1.0	43.0	-	-		-	-	.124	-	-
			1.0	43.3	-	-		-	-	.108	-	-
		N_2	0.1	40.5	-	-		-	-	.043	-	-
			0.3	42.3	-	-		-	-	.066	-	-
			1.0	40.7	-	-		-	-	.068	-	-
		He	0.1	40.8	-	-		-	-	.046	-	-
			0.3	36.2	-	-		-	-	.068	-	-
			1.0	36.6	-	-		-	-	.089	-	-
	Epoxy	Air	0.1	42.0	-	-	2	-	-	.213	-	-
			0.3	41.0	-	-		-	1.13	.179	-	-
			1.0	42.0	-	-		-	1.45	.239	-	-
		N_2	0.1	40.0	-	-		-	-	.238	-	-
		N_2	0.3	39.0	-	-		-	1.33	.159	-	-
		He	0.1	40.0	-	-		-	1.33	.161	-	-
		He	0.3	37.0	-	-		-	1.18	.142	-	-
	PBI	Air	0.1	40.0	-	3110	2	-	.410	.056	34.4	-
	PEI	N_2	0.1	41.0	-	3150	2	-	.410	.081	28.2	-
	Elastomer	Air	0.1	42.0	-	-	2	-	1.270	.192	-	-
	Elastomer	N_2	0.1	40.0	-	-	2	-	1.270	.252	-	-

Table 1.- Concluded.

Facility	Material	Test gas	Pressure, atm	Heat flux, MW/m^2 Measured	Heat flux, MW/m^2 Corrected	Surface temperature, K	Test time, s	Δx, cm	$\Delta \ell$, cm	Δm, gm	E, MJ/kg	E^c, MJ/kg
Carbon arc	LDPN	Air	0.3	33.4	12.3	3213	5	.050	.305	.064	83.4	20.4
			1.0	40.3	14.8	3203		.050	.406	.083	78.2	21.2
			3.0	35.5	13.1	3113		.030	.356	.070	78.4	21.2
			3.0	34.7	12.8	3043		.030	.305	.084	90.4	25.0
		N_2	1.0	39.0	14.3	3163		.050	.305	.073	101.0	27.5
		He	1.0	37.7	13.9	3173		.050	.330	.077	89.6	24.0
		CO_2-N_2	1.0	30.4	11.2	2993		.050	.279	.051	85.7	23.1
		CO_2-N_2	3.0	32.9	12.1	3113		.100	.305	.071	83.8	25.8
	Epoxy	Air	1.0	33.4	12.3	3043	5	.040	.660	.090	43.1	11.8
	Epoxy	CO_2-N_2	3.0	35.5	13.1	2823	5	.290	.587	.090	53.9	16.4
	Elasto-mer	Air	1.0	33.4	12.3	3003	5	.870	1.14	.069	53.4	14.9
		Air	3.0	36.0	13.2	3003		.870	1.55	.069	42.6	12.0
		CO_2-N_2	3.0	33.8	12.4	3023		.770	1.12	.062	54.9	15.2
	P-1	Air	1.0	32.1	11.8	3073	5	.280	.406	.047	56.6	14.8
	P-2			33.4	12.3	3153		.050	.508	.040	41.1	10.5
	P-3			37.4	12.8	3093		.070	.381	.035	82.1	22.1

Table 2.- Graphite Test Results

Facility	Test gas	Pressure, atm	Heat flux, MW/m^2		Surface temperature, K	Test time, s	Δx, cm	Δm, gm
			Measured	Corrected				
Laser	Air	0.1	42.0	-	3615	5	.203	.073
		0.1	42.0	-	3619		.204	.073
		0.3	42.0	-	3530		.191	.069
		0.3	42.0	-	3400		.186	.067
		1.0	45.8	-	3345		.203	.073
		1.0	44.2	-	3345		.185	.067
	N_2	0.1	40.0	-	2900	5	.102	.006
		0.1	41.6	-	2865		.102	.005
		0.1	45.8	-	2860		.102	.004
		0.1	47.0	-	2850		.110	.008
		0.3	42.1	-	2865		.102	.006
		0.3	41.4	-	3080		.089	.005
		1.0	42.0	-	3500		.110	.020
		1.0	40.8	-	3400		.102	.016
	He	0.3	39.2	-	-	5	.102	.011
		0.3	37.7	-	2650		.089	.004
		1.0	38.0	-	3080		.102	.011
		1.0	38.8	-	3185		.114	.012

Table 2.- Continued.

Facility	Test gas	Pressure, atm	Heat flux, MW/m^2		Surface temperature, K	Test time, s	Δx, cm	Δm, gm
			Measured	Corrected				
Carbon arc	Air	0.3	37.2	13.7	3600	5	0	.005
		1.0	42.5	15.6	3800			.008
			35.5	13.1	3690			.003
			32.5	12.0	3540			.003
			34.1	12.5	3590			.005
			34.0	12.5	3600			.004
			27.4	10.1	3070			.004
			32.0	11.8	3540			.006
		3.0	34.2	12.6	3490			.011
			33.4	12.3	3400			.005
			30.4	11.2	3500			.004
			34.9	12.8	3440			.006
		5.0	34.9	12.8	3580			.010
			38.7	14.2	3740			.010
			35.7	13.1	3590			.011
			34.7	13.8	3800			.010
		8.0	28.8	10.6	2880			.014
			32.4	12.0	3240			.014
			30.0	11.0	3000			.015
			31.8	11.7	3180			.013

Table 2.- Concluded.

Facility	Test gas	Pressure, atm	Heat flux, MW/m^2		Surface temperature, K	Test time, s	Δx, cm	Δm, gm
			Measured	Corrected				
Carbon arc	CO_2-N_2	1.0	32.0	11.8	3370	5	0	.004
		3.0	37.6	13.8	3680			.006
		3.0	38.2	14.0	3650			.005
		5.0	34.5	12.7	3760			.010
		5.0	33.5	12.3	3700			.009
		5.0	33.0	12.0	3670			.010
		5.0	29.7	11.0	3300			.006
Xenon arc	Air	1.0	11.5		2650	10	.008	.103
					2800	20	.018	.159
					2600	20	.018	.325
					2850	30	.024	.220
					3000	30	.025	.129
			10.0		2600	30	.020	.207
			10.0		2800	60	.039	-

Table 3.- Low-Density Phenolic Nylon Calculations

Facility	Test gas	Pressure, atm	Heat flux, MW/m^2	Time, s	$\Delta\ell$, cm		Δx, cm	
					Calculated	Experimental	Calculated	Experimental
Carbon arc	Air	0.3	33.4	5	.585	-	.329	-
		0.3	12.3[c]		.407	.305	.012	.05
		1.0	40.3		.667	-	.459	-
		1.0	14.8[c]		.428	.406	.029	.05
		3.0	35.5		.607	-	.367	-
		3.0	13.0[c]		.413	.356	.015	.03